Universitat Autònoma
de Barcelona

A thesis for the

Master in Telecommunications Engineering

Synthesis Considerations for Acoustic Wave Filters and Duplexers Starting with Shunt Resonator

Eloi Guerrero Menéndez

eloi.guerrero@uab.cat

SUPERVISOR: Pedro de Paco Sánchez

pedro.depaco@uab.cat

Department of Telecommunications and Systems Engineering

Universitat Autònoma de Barcelona (UAB)

Escola d'Enginyeria

January, 2020

El sotasignant, Pedro de Paco Sánchez, Professor de l'Escola Tècnica Superior d'Enginyeria (ETSE) de la Universitat Autònoma de Barcelona (UAB),

CERTIFICA:

Que el projecte presentat en aquesta memòria de Treball Final de Master ha estat realitzat sota la seva direcció per l'alumne Eloi Guerrero Menéndez.

I, perquè consti a tots els efectes, signa el present certificat.

Bellaterra, 24 de gener de 2020.

PEDRO ANTONIO DE PACO SANCHEZ

Digitally signed by PEDRO ANTONIO DE PACO SANCHEZ
Date: 2020.01.22 18:39:23 +01'00'

Signatura: Pedro de Paco Sánchez

Resum:

La complexitat de les capçaleres de radiofreqüència per telefonia mòbil s'ha incrementat en pocs anys i un dels elements més importants dins d'aquestes són els filtres. Aquests dispositius són els responsables del correcte funcionament de la comunicació en el paradigma actual d'un espectre radioelèctric massivament ocupat. La implementació de més de 25 filtres en un mateix terminal mòbil es veu impulsada per l'ús de la tecnologia d'ona acústica.

Aquest projecte presenta una metodologia de síntesi de filtres i duplexors d'ona acústica en topologia d'escala tenint també en compte el cas de les xarxes que comencen amb un ressonador en paral·lel. La viabilitat d'aquestes xarxes s'investiga en termes de la fase de la funció de filtrat i s'aporta una visió de síntesi pas baix de les limitacions que poden aparèixer, proveint alhora diferents solucions perquè els dissenyadors puguin obtenir xarxes viables.

Resumen:

La complejidad de los cabezales de radiofrecuencias de telefonía móvil ha aumentado exponencialmente en pocos años y uno de los elementos más importantes dentro de estos son los filtros. Estos dispositivos son los responsables del correcto funcionamiento de la comunicación en el actual paradigma de espectro radioeléctrico masivamente ocupado. La implementación de más de 25 filtros en un mismo teléfono móvil se ve impulsado por el uso de la tecnología de onda acústica.

Este proyecto presenta una metodología de síntesis de filtros y duplexores de onda acústica de topología en escalera considerando también el caso de redes cuyo primer resonador está conectado en derivación. La viabilidad de estas redes se investiga en términos de la fase de la función de filtrado y se aporta una visión de síntesis paso bajo de las limitaciones que pueden aparecer, proveyendo diferentes soluciones para que los diseñadores puedan conseguir redes viables.

Summary:

The complexity of radio frequency front-end modules in mobile phones has increased exponentially in a few years and one of the most important devices within these are filters. The devices responsible for the correct performance of communication in the current paradigm of massively occupied spectrum. The implementation of more than 25 of these devices in a single mobile phone is leveraged in the use of acoustic wave technology.

This project presents a synthesis procedure for acoustic wave ladder filters and duplexers taking also into consideration the case of networks whose first resonator is in shunt configuration. The feasibility of these networks in terms of the phase of the filter function is investigated and a lowpass synthesis view of the issues that might arise is presented providing different approaches for designers to achieve feasible networks.

Contents

List of Figures

List of Tables

Chapter 1

Introduction

Radio frequency (RF) filters constitute a fundamental part of any communications system involving electromagnetic waves. The essential function of selecting the desired portion of the spectrum and rejecting all adjacent signals is even more important in the current paradigm of massive spectrum occupancy driven by the needs of an ever-increasing mobile communications market. Any new release by 3GPP[1] introduces new bands - placed either above, below and in-between the current spectrum allocations - that are closer one from each other. For example, Long Term Evolution-Advanced Release 14 (referred as LTE-A Pro) defined 44 mobile communication bands and allowed up to 32 aggregated carriers.

An increase in communication capacity, transfer velocity or latency reduction, among others, are service advances that are also tightly connected to the performance specifications of all devices within new systems: steep skirts, high selectivity and low insertion losses, among others. Notice for example the concept of carrier aggregation (CA): achieving an effective larger bandwidth (and thus, larger capacity) by jointly processing the content of multiple smaller bandwidth channels. This concept invalidates the simple approach of band selection by using a switching device among different duplexers. On the contrary, it leads the development of multiplexer filter solutions [5], increasing design complexity but also allowing more compact devices.

Not only more bands are available, but also their deployment is not the same in every region. LTE bands in America are not the same as in Europe or Asia. As worldwide mobility is now common, it is desired that all mobile phones are capable of operating in every region and this increases the amount of filters that a single phone must implement. Nowadays, phones feature more than 25 filters distributed along legacy GSM and UMTS bands, current LTE-A

[1] 3rd Generation Partnership Project.

Pro and upcoming 5G New Radio, besides GNSS[2], WiFi and Bluetooth.

At the same time than an issue of complexity of the RF front-end module (FEM), RF filtering also becomes an issue of volume. As hand-held devices shrink in size and thickness driven by consumer demands, internal circuitry must also reduce its size. This is not a trivial issue from the filter point of view. Filters are devices made of resonators and the microwave knowledge dictates that sizes are of importance when designing them: $\lambda/4$ and $\lambda/2$ structures are the basic building blocks. Considering that the operating bands are in the vicinity of 3 GHz, the wavelength at these frequencies will span from 10 to 70 centimetres approximately. It is obvious that fitting more than 25 filters inside a mobile phone is, at best, not an easy task. An initial guess might think in microstrip designs on high dielectric permittivity (ε) substrates to reduce the effective wavelength, but the quality factor (Q) of microstrip technology is too low for applications in need of low losses and high selectivity. In turn, acoustic wave technology is capable of fulfilling performance specifications (e.g. quality factors above 1000, steep skirts, low insertion loss) while keeping the size of the device in the microscopic world. This is possible because the filtering behaviour takes place in the acoustic domain thanks to the piezoelectric effect, as will be explained in the following chapter.

1.1 Historical Perspective of Mobile Phone Filters

The DynaTAC 8000x by Motorola was used in 1973 in the first mobile phone call in history and ten years later, was made commercially available [6]. It featured operation at a single band and the filtering stage at the RF-FEM was a ceramic duplexer with 869-894 MHz transmitter (TX) and 824-849 MHz receiver (RX) channels. The phone was bulky and weighted more than 800 grams but at the beginning of mobile telephony, size and weight were not an essential concern.

At the same time, advances in surface acoustic wave (SAW) resonator filters were published and the first filter designs at the UHF band were proposed [7]. The development of SAW resonator technology in the scope of filtering devices was leveraged on its initial role in the design of oscillators and pulse compressors for radar systems. Since then, SAW technology has become a key factor in the mobile phone industry. Its role in the market is still strong, but until the end of the 90's decade it had a dominating market position. In parallel to SAW, the bulk acoustic wave (BAW) technology was being developed and the first BAW resonators were demonstrated [8]. At first it was not clear that BAW could commercially compete against SAW filters that were already in high-volume production. However, in 1998 the BAW team at

[2]Global Navigation Satellite System.

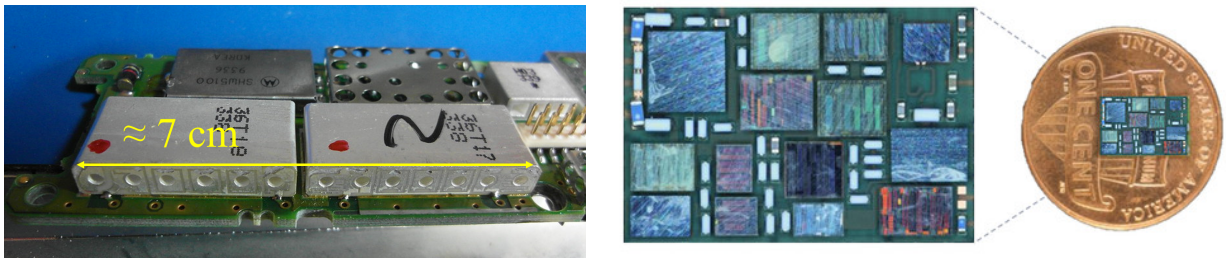

(a) (b)

Figure 1.1: Mobile phone filters evolution (a) Ceramic duplexer of the Motorola DynaTAC 8000x (b) 2016 filter module by Qorvo featuring 16 SAW filters in a 45 mm^2 die.

Hewlett Packard Laboratories fabricated the first BAW duplexer [9] for mobile phones, connected it to a terminal and used it to call their managers. This novel duplexer at 1900 MHz (PCS-CDMA[3]) got rid of a large ceramic duplexer and was strongly supported by the industry. This supposed a major leap forward in the role of acoustic wave technology in the mobile communications sector.

Since then, innovation in acoustic wave filters has increased and nowadays, both SAW and BAW are responsible for the RF filtering stages in our phones. The predominance of one type of acoustic resonator over the other has sometimes been predicted but reality is that both have defined application spaces. A graph distributing acoustic wave technologies in terms of complexity and working frequency can be found in [4]. In recent years, new manufacturing processes, materials with enhanced capabilities and novel topologies have been proposed and suppose a sign of vitality of this field that is of great interest to the industry.

1.2 Network Synthesis Approach for Acoustic Wave Filters

The increasing demand of more LTE or 5G bands incorporated in a single smartphone drives mobile phone industry players towards the shrinkage of RF FEMs to even smaller sizes and the manufacture of joint RF modules including power amplifiers, switches and filters. This is a clear message of the bright future of RF acoustic wave technologies but also an indication that the specifications demanded to this technology increase in complexity. To fulfil present specifications and be able to develop future solutions, the filter design methodology must be carefully considered as it will boost or hinder the performance of the company.

In [4], a detailed description of the design process is given. It can be mainly divided among

[3]Personal Communications Service - Code Division Multiple Access.

two approaches: starting an optimization procedure on an already marketed filter aiming to fulfil newer specifications might be the simpler case and the one involving less time to market. On the other hand, the common practice is to devise a primary look of the filter, arranging resonators and setting primary optimization goals such as the transfer function, return loss or total area occupancy, and start an optimization procedure. At each iteration, the output might be a filter or not, and among those that are, more specifications must be imposed such as the effective coupling constant homogeneity or even non-linear effects. Although this method has proven effective for the industry, from a performance point of view, note that many optimization steps might not be useful since their output might not even be a proper filter response, and on top of that, the fact that the filter network is obtained from optimization entails a loss of control on the network itself. This might lead to problems during further optimization procedures.

The objective behind this thesis is to shed some light on how to control the initial stages of acoustic wave filter design by means of a synthesis procedure. Synthesizing means computing which elements compose the filter starting from the definition of a desired transfer function. This approach provides a controlled point of view of both the network and the role of each of the elements, and is opposite to a hard optimization effort made on an arbitrary arrangement of resonators. This does not imply that all synthesized filters will be manufacturable in terms of acoustic wave technology, but ensuring that every execution of the procedure will output a filter is a major advance. This will allow to apply search methodologies based on optimization algorithms to find a filter fulfilling all the required technological constraints and/or response specifications. Not an uncontrolled optimization but rather a directed search among all possible solutions.

Network synthesis procedures have been a topic of interest for years, many advances are still possible and it was not until [3] that the acoustic technology and the synthesis worlds were connected. In this thesis, apart from presenting the reasoning behind the synthesis procedure, the specific case of acoustic wave filters starting with shunt resonator is covered to provide some general design considerations.

1.3 Thesis Outline

After this short initial chapter of introduction to the mobile phones filtering market and the motivations behind the synthesis method presented in this thesis, the remaining content is divided in four chapters.

Chapter two is dedicated to the presentation of acoustic wave technology. The piezoelectric

effect, types of acoustic wave propagation and their associated resonant structures, SAW and BAW, are presented and after that the electrical model that describes this resonators, the Butterworth - Van Dyke, is introduced. Finally, the different classes of acoustic wave filters are briefly described, paying more attention to the ladder topology that is the one considered in this thesis.

The third chapter covers all aspects related to the synthesis of acoustic wave filters. Initially, a brief introduction to the two main synthesis procedures is given and after that, the computation of the Generalized Chebyshev filter function is carefully described. After this, the lowpass equivalent model of acoustic resonators and the lowpass prototype network to be synthesized are presented. In this chapter the role of input and output reactive elements in acoustic wave ladder filters and their relation with the input phase are also discussed. Finally, the synthesis methodology is described including the case of duplexers and to close the chapter, a duplexer example is provided.

The fourth chapter describes the approach to the synthesis of ladder filters whose first resonator is in shunt configuration and introduces the issues that might arise when dealing with them. Solutions to these issues are discussed from a synthesis point of view.

Finally, chapter five includes the conclusions to this work and open topics still to be researched.

Chapter 2

Basics on Acoustic Wave Technology

This chapter introduces the basic concepts of acoustic wave (AW) technology and its application to microwave devices. Types of resonators, materials used in manufacturing, filter topologies and other physical parameters of importance are covered.

2.1 Acoustic Waves and Piezoelectricity

It has been mentioned in the introduction that acoustic wave filters can be implemented in microscopic sizes because the filtering action happens in the acoustic domain. This means that the electromagnetic (EM) wave to be filtered is transformed into a mechanical wave propagating through a material. The propagation velocity of the acoustic wave in the material is much lower than the electromagnetic propagation velocity in vacuum and since the frequency is unaltered, the resulting acoustic wave has a micron-order wavelength. Thus, structures of λ-like dimensions do not become privative in terms of space and resonant structures can be implemented.

Before focusing in the device itself, it is interesting to comment how do EM waves transform to acoustic. This is a transduction process (i.e. a transformation of energy from one nature to another) that in this case is mandated by the piezoelectric effect. Piezoelectricity is a characteristic that refers to the capability of a material of transforming an applied strain or pressure to an electric field. The inverse piezoelectric effect corresponds, consequently, to the transformation of an applied electric field into a deformation of the material. This effect are described by the following equations from [10], where T is stress in $[N/m^2]$, S is strain, c^E is

mechanical stiffness in $[N/m]$, e is the piezoelectric coefficient in $[m/V]$, ε^E is permittivity in $[F/m]$, E is the electric field in $[V/m]$ and D is the displacement current in $[A]$. Superscripts in constants indicate that they are evaluated under specific conditions, namely constant electric field or constant stress.

$$T = c^E S - eE \tag{2.1}$$

$$D = eS + \varepsilon^S E \tag{2.2}$$

The first equation is a modification of the traditional Hooke's law to account for the effect on stress of an external electric field. The second equation decribes how stress has an effect on electrical displacement. Therefore, the above equations describe how the mechanical and electrical properties of the material are coupled and it is clear then, that an electromagnetic field will induce a mechanical wave if applied to a piezoelectric plate. However, the application of an EM field (or equivalently a voltage) to the plate can be approached in many ways and will define, jointly with the physical dimensions of the plate, how do the induced waves propagate. For the purpose of this thesis the two main propagation cases will be considered, the surface acoustic wave (SAW) and the bulk acoustic wave (BAW).

2.1.1 Surface Acoustic Wave

SAW is a wave that propagates along the surface of the piezoelectric plate. Induction of such wave is possible by means of metallic interdigital transducers (IDT) deposited on the material. The length and separation of the electrodes in the propagation direction will define the working frequency of the transducer, being $\lambda/4$ the typical length. Figure 2.1 depicts a SAW resonator with IDTs. To create a resonant structure, input and output IDTs and additional side reflectors to create reflection back to the transducers are used. Note that the thickness of the piezoelectric plate is much larger than the distance between electrodes to ensure that only SAW modes propagate. Controlling which modes propagate through the structure is important to avoid parasitic resonances and response ripples.

The frequency of operation of SAW resonators has traditionally been limited by integrated circuit (IC) manufacturing capabilities as the frequency is defined by the IDT electrodes. The common commercial upper frequency limit for SAW is located at 2.5 GHz as it would require lithography resolution below 0.25 μm what would suppose an undue manufacturing effort. One of the merits of SAW is that the manufacturing process is simpler than BAW as it can commonly be approached as a single layer single mask process. An important feature of

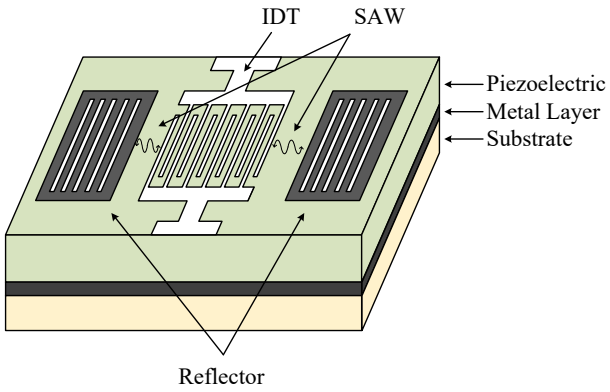

Figure 2.1: Structure overview of a SAW resonator

resonators is its achievable quality factor (Q), that for SAW can be considered at around 1300 [11].

In terms of materials, SAW resonators are commonly manufactured using Lithium Niobate ($LiNbO_3$) or Lithium Tantalate ($LiTaO_3$) plates [12]. An important feature of piezoelectric materials in the RF domain is the temperature coefficient of frequency (TCF) measured in ppm/°C. This is a measure of how the resonance frequency of a resonator drifts as temperature increases. TCF is computed as

$$TCF = -TEC + TCV \tag{2.3}$$

where TEC is the temperature expansion coefficient and TCV is the temperature coefficient of velocity. $LiNbO_3$ and $LiTaO_3$ have positive TEC and negative TCV, what yields a common measure of -30 to -40 ppm/°C TCF. In applications with more stringent temperature conditions, for example in duplexers, temperature compensation techniques (TC-SAW) have been developed to counter the negative TCF by for example depositing Silicon Oxide (SiO_2) over the electrodes achieving a TCF around -10 ppm/°C.

2.1.2 Bulk Acoustic Wave

As the term indicates, BAW is a wave that propagates through the bulk of the piezoelectric material. Therefore, the design dimension to consider for a resonant structure will be the thickness of the plate and its relation to the wavelength. The fundamental resonance of BAW devices is found when the thickness of the resonator (electrodes included) is half an acoustic wavelength. BAW resonators are built as a sandwich of a piezoelectric material between metallic electrodes that are mostly made of Molybdenum (Mo) or Tungsten (W) [11]. In terms of the piezoelectric material, the most used for BAW is Aluminium Nitride (AlN) but also Zinc

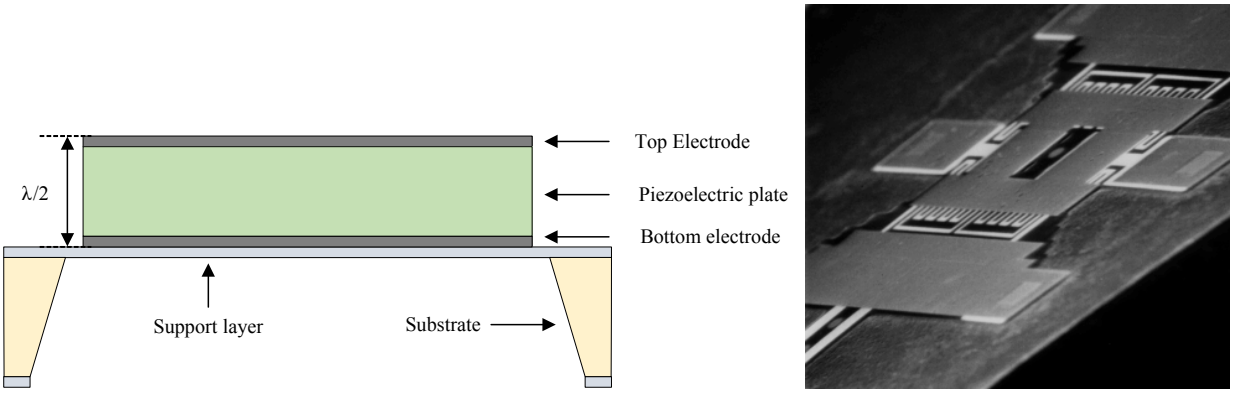

Figure 2.2: FBAR resonator technology. (a) Cross-section of an FBAR resonator, (b) SEM image of a manufactured "air-bridge" FBAR resonator [1].

Oxide (ZnO), Cadmium Sulfide (CdS) or even Lead Zirconate Titanate (PZT) resonators can be found in the literature even though they are not currently a commercial alternative due to losses at high frequencies and other manufacturing limitations.

As seen with SAW, an essential feature to achieve an acoustic resonant structure is finding a way to confine the acoustic wave in the resonator. In the case of BAW, the implementation of reflective boundaries above and below the resonator electrodes could be ideally achieved by ensuring top and bottom air interfaces as air acts as a short circuit in the acoustic domain. Given this, BAW resonators can be divided among two main types for simplicity in this description. The first type is the film bulk acoustic resonator or FBAR, that consists in confining the acoustic wave by manufacturing an air cavity below the resonator, as shown in the cross-sectional view in Figure 2.2a. As the cavity isolates the substrate from the resonator, losses are reduced, but construction of the cavity is not an straightforward task. Initially, the pothole membrane process was used but novel methods have been developed by the industry such as the undercut air gap membrane described in [10]. Figure 2.2b shows the scanning electron microscope (SEM) image of a manufactured FBAR resonator.

The second BAW resonator is the solidly mounted resonator or SMR. In this case the bottom reflection condition is achieved via a disposition of multiple $\lambda/4$ layers of alternating high and low impedance composing a Bragg reflector. The reflector layers can be achieved, for example, by alternate deposition of metal and oxide membranes. Figure 2.3a depicts the cross-section view and figure 2.3b shows a SEM image of an SMR resonator. Due to the fact that the resonator is actually in contact with the substrate and that the Bragg reflector has a limited operation bandwidth, energy in undesired parasitic modes can scape the resonator and thus increase losses. However, a solution can be attained by careful optimization of the

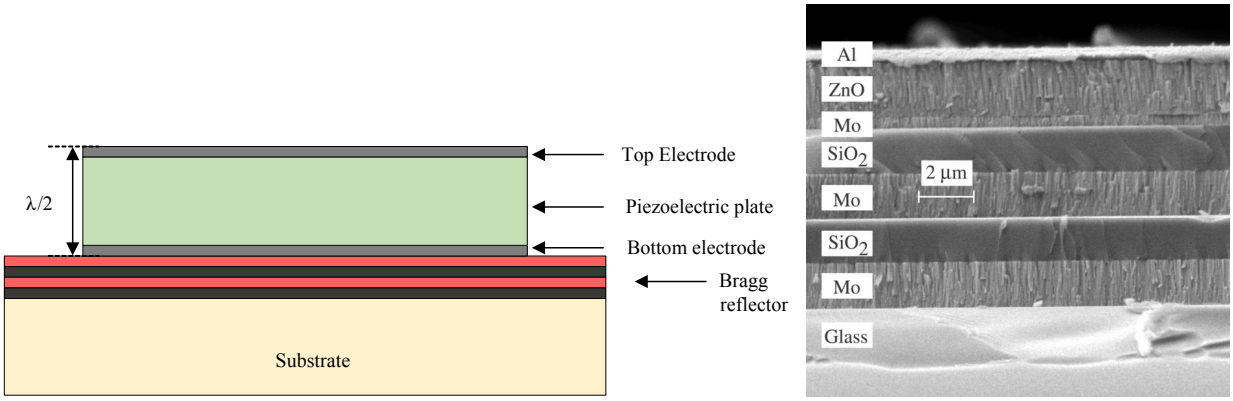

Figure 2.3: SMR technology. (a) Cross-section of an SMR, (b) SEM image of a manufactured ZnO SMR [2].

reflector layers not only at the main resonance frequency but also at the shear mode frequency. The presence of this reflector is the reason why SMR resonators have a slightly lower Q factor than FBAR. The common measure is a maximum achievable Q of 3000 and 5000 respectively [11]. On the contrary, thanks to the Bragg reflector, the power handling capabilities of SMR are better than FBAR. The actual connection of the resonator to the substrate acts as a sink for the cumulated heat while in FBAR, only the edge supports that hold the resonator can act as heat dispersers.

2.2 Electrical Modelling of Acoustic Wave Resonators

To face the design of resonators and consequently, filters, it is important to obtain an equivalent circuit model that represents the behaviour of the acoustic resonator and allows a certain level of abstraction from the physics involved in it. To begin with, let us consider in (2.4) the input impedance expression of an acoustic resonator considering only the fundamental mode as proposed in [10], being C_0 the static capacitance, C_a the motional capacitance and L_a the motional inductance.

$$Z_{in}(\omega) = \frac{j\left(\omega L_a - \frac{1}{\omega C_a}\right)}{1 - \omega^2 C_0 L_a + \frac{C_0}{C_a}} \tag{2.4}$$

It can be seen that an acoustic resonator shows two resonances: a series resonance frequency f_s where its impedance tends to zero and an anti-resonance frequency (also, parallel) f_p where its impedance tends to infinity. The three reactive elements in the expression above

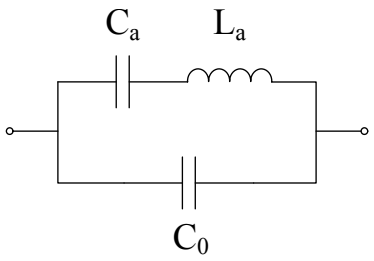

Figure 2.4: Butterworth - Van Dyke model of an acoustic resonator

conform the well-known Butterworth - Van Dyke (BVD) model for acoustic resonators shown in Figure 2.4. The so-called static capacitance C_0 accounts for the natural capacity created between electrodes (either the parallel plates of BAW or at the IDT in SAW) and the two motional elements C_a and L_a model the resonance due to confinement of the acoustic wave.

The two resonances that have been mentioned can be easily computed as

$$f_s = \frac{1}{2\pi\sqrt{L_a C_a}} \tag{2.5}$$

and

$$f_p = \frac{1}{2\pi}\sqrt{\frac{C_a + C_0}{L_a C_a C_0}} = f_s\sqrt{1 + \frac{C_a}{C_0}} \tag{2.6}$$

Notice also that as the capacitance ratio C_a/C_0 will always be a positive number, the resonance frequency will always be below the anti-resonance. Figure 2.5 depicts the input impedance of an acoustic resonator both in magnitude and phase. Notice that the resonator is intrinsically capacitive (showing a phase of -90^{o}) at frequencies not between the two resonances because of the predominant role of C_0, but becomes inductive (phase of 90^{o}) between resonances.

Two aspects are worth being mentioned. The simplification to only the fundamental mode in the input impedance mandates that a single motional arm is present in the BVD model. If higher order modes are considered, the BVD model also accounts for them by adding more motional branches in parallel. Whereas, closed expressions relating the BVD elements and the physical properties of an acoustic resonator exist for the two types of resonators. In the case of BAW, for example, the static capacitance can be computed with the common expression,

$$C_0 = \frac{\varepsilon^s A}{t} \tag{2.7}$$

being A the area, ε^s the permittivity and t the thickness of the resonator. On the other hand, the motional arm elements are defined by k^2_{eff}, the effective electromechanical coupling factor,

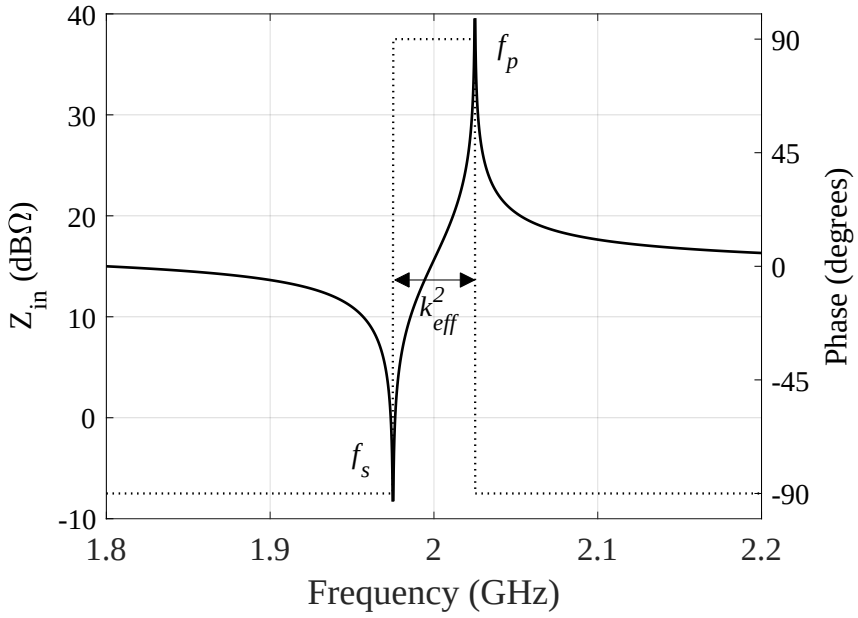

Figure 2.5: Input impedance (magnitude and phase) of an acoustic resonator

that is an important parameter describing how electrical energy is transformed to mechanical energy and vice versa, for a given resonator model. This parameter is related to the original electromechanical coupling coefficient (K^2) shown in [10] that is a function of stiffness, the piezoelectric constant and permittivity, but in this case is computed as follows.

$$k_{eff}^2 = \frac{\pi}{2}\frac{f_s}{f_p}\cot\left(\frac{\pi}{2}\frac{f_s}{f_p}\right) \tag{2.8}$$

A value of K^2 will define the maximum achievable k_{eff}^2 using a given material, but much lower values can be achieved due to incorrect design of the resonator. As an example, a common measure for achievable k_{eff}^2 in BAW is 6.5% for AlN and 8.5% for ZnO. However, these values can be slightly different among competitors in the industry. Assessing how the effective coupling coefficient is affected by the construction of a the resonator falls out of the scope of this thesis, but further studies can be found in [10, 13]. Given this effective coupling coefficient, the motional elements of the BVD are computed as in [14], where v is the sound propagation velocity in the piezoelectric material and N is the acoustic mode.

$$\frac{C_a}{C_0} = \frac{8k_{eff}^2}{N^2\pi^2} \qquad \text{and} \qquad L_a = \frac{v}{64 f_s^3 \varepsilon A k_{eff}^2} \tag{2.9}$$

In terms of quality factor of the resonator, the BVD model proposed above does not account for losses but a modified version of it (thus called the modified BVD or mBVD) was presented in [15] including resistors to model the material, electric and acoustic losses at the two resonances. Commonly, the quality factor of the two resonances is not exactly the same but can be assumed equal for simplicity.

As commented at the beginning, the use of models is interesting to reduce simulation and optimization complexity in the design procedure. As the BVD model describes the electrical behaviour of the resonator considering the limitations mentioned above, from an acoustic domain point of view other models can be used to describe the propagation of acoustic waves in an accurate manner. The Mason model [16] was proposed in 1951 and is the most common approach for BAW resonators. It is a one-dimensional structure that comprises an electroacoustic transducer by means of a transformer and transmission lines to model acoustic propagation. This model is useful to, for example, describe the interaction of layers in the Bragg reflector of SMR resonators. Unfortunately, the Mason model is not applicable to SAW devices but the analysis of wave propagation in the IDT structure is possible by means of the P-matrix [17]. This matrix is a 3-port mathematical tool derived from the Coupled Mode theory that describes the coupling between electric fields and acoustic waves in the IDT. Several P-matrices for the different fingers can be cascaded to model the entire device.

2.3 Acoustic Wave Filter Topologies

Several types of filters constituted by acoustic wave resonators exist and can be divided between two main classes with respect to their coupling mechanism: electrically connected or acoustically coupled filters. Note that the difference resides in which is the domain at which the coupling between resonators is made. Electrically connected filters include ladder and lattice filters while stacked crystal filters (SCF) and coupler resonator filters (CRF) belong to the acoustically coupled group.

In the mobile phone market the most important topologies are the ladder one, both in SAW and BAW, and also CRF in SAW. The lattice type was initially given a bright future as it is a balanced structure and balanced-input integrated circuits (IC) were being manufactured at that moment, but the ladder type has landed as the common choice. This thesis covers the synthesis of ladder filters and therefore these will be the ones explained in this section. Further knowledge on the other topologies can be found in [10, 13].

2.3.1 Ladder-type Acoustic Filters

The ladder acoustic filter is an inline topology composed of consecutive series and shunt resonators conforming the so-called ladder. Input and output reactive elements are needed in this topology. Their paper will be deeply discussed in the following chapter from a synthesis point of view. Figure 2.6 shows the classical schematic of a ladder filter. It is worth comment-

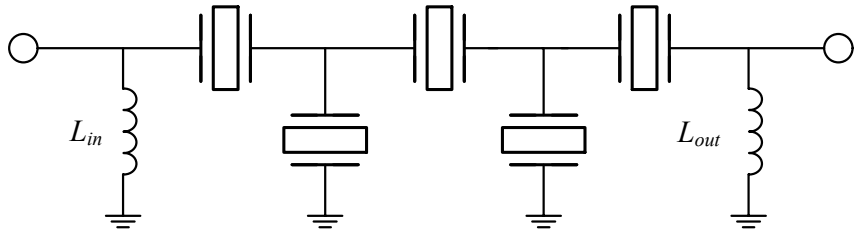

Figure 2.6: Acoustic wave ladder 5th-order filter topology overview.

ing that not only resonators in shunt or series configuration can be present in the topology. Some ladder filters, at the beginning, featured capacitors in some shunt branches as a means to couple two series resonators [10].

Figure 2.7 shows a classical plot extracted from [3] to explain the working principle of the acoustic ladder filter. It has been shown that acoustic resonators feature two resonances: series ($Z_{in} = 0$), and parallel ($Z_{in} = \infty$). Therefore, at the series resonance frequency of a shunt resonator (let it be f_s^{SH}) the impedance of this resonator will be ideally zero and create a short circuit path to ground, thus implementing a transmission zero (TZ) at finite frequency. Similarly, at the parallel resonance frequency of a series resonator (f_p^{SE}) the impedance of the resonator will be ideally infinite imposing an open circuit in the main path of the filter and hence implementing a finite transmission zero. As shown in 2.6, f_p will always be above f_s and therefore, to create a filter, shunt resonators will implement TZs below the passband and series resonators will place them above. The series resonance of series resonators f_s^{SE} and the parallel resonance of shunt resonators f_p^{SH} will always be placed inside the passband and will ensure that the signal can propagate from input to output. It has been stated before that between resonances, the acoustic resonator is inductive what means that the input phase of the filter inside the passband will have a positive slope. This is an important observation that will be exploited in forthcoming chapters.

We have shown before that far from the resonances, the acoustic resonator has a capacitive behaviour dominated by the static capacitance C_0. Hence, the out-of-band (OoB) rejection of a ladder filter comes defined by the capacitive voltage divider made of the static capacitances of all resonators. This poor OoB rejection level is one drawback of ladder filters, but can be tackled by the addition of external elements in the substrate of the device [18]. In the in-band region, the passband and its associated return loss are formed by the superposition of the reactive parts of all resonators. In general, it is clear that thanks to the implementation of transmission zeros, filters with steep skirts can be manufactured at the expense of a poorer OoB rejection. The rejection level increases with the order of the network (the capacitive divider becomes larger) but at expense of increased insertion losses. This defines a trade-off

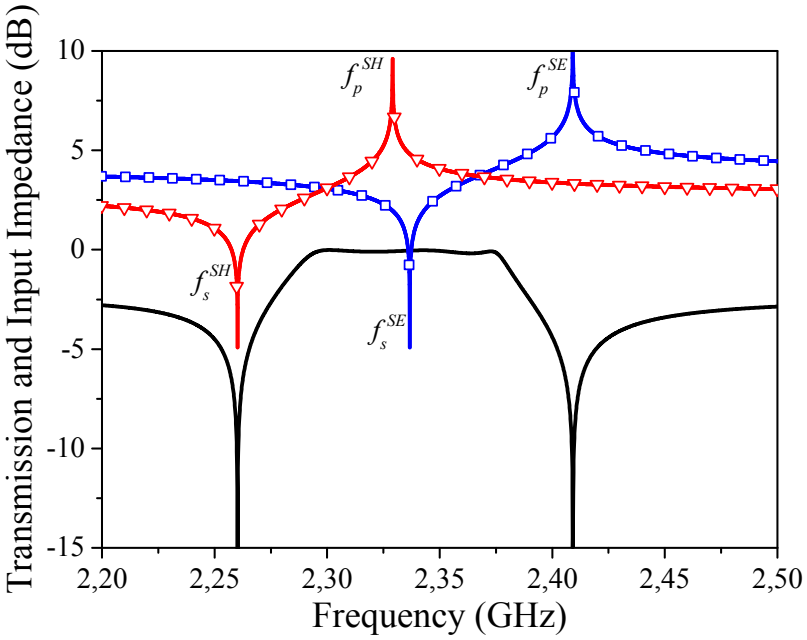

Figure 2.7: Working principle of a second order AW ladder filter [3].

that is important in the mobile phone market due to the need of reducing battery consumption. 7th order filters are common in the current product portfolio but companies are already developing 9th order solutions.

It is important to point out the strong role of the effective coupling coefficient k^2_{eff} of the resonator in the definition of the filter bandwidth. We have shown in 2.8 that k^2_{eff} is related to the distance between resonances (also, pole-zero distance). Considering that a single piezoelectric material can be used in the manufacture of a filter, the maximum achievable coupling coefficient is therefore bounded, and so does the maximum achievable bandwidth. A common measure is that the achievable fractional bandwidth is around half the effective coupling coefficient [13]. However, the use of external reactive elements allows to implement effectively larger or even smaller values of coupling coefficient while ensuring feasibility of the filter. This extent is explained in [19].

From a network point of view, the one addressed in the following chapters, the ladder filter is a fully canonical network. This means that it has as many resonators as transmission zeros. Moreover, this is a network where each of the transmission zeros is independently implemented by one of the resonators. This feature allows the use of extracted pole techniques for the synthesis of ladder filters.

Chapter 3

Synthesis of Acoustic Wave Ladder Filters

As opposed to network analysis, the process of mathematically solving a circuit to obtain its response, network synthesis is the mathematical process of obtaining the elements and their disposition, to implement a desired response defined by a function. This is not a trivial problem and many contributions have been done during more than 80 years. The current state of filter synthesis techniques is summarized in the reference book by Cameron, Kudsia and Mansour [20].

This chapter covers the synthesis procedure of filter networks composed of acoustic wave resonators. At first, an overview of the available synthesis techniques for microwave filters is provided and the most common filtering functions are presented. The Generalized Chebyshev function and the method to compute it are explained in deep, and then, it introduces a low-pass nodal model for the acoustic ladder topology and an extracted-pole synthesis method. The strong role of the input phase throughout the process is also examined and a duplexer synthesis example is provided at the end of the chapter.

3.1 Network Synthesis Methods

Aiming to translate a filter function to a prototype electrical circuit from which the actual microwave filter can be derived, two fundamental synthesis techniques exist in the literature. They are, the circuit synthesis approach that is based on the $ABCD$ matrix, also called *chain* matrix, and the direct coupling matrix synthesis approach. Both of them start by the definition of a filter function in the lowpass domain and their output is a prototype circuit composed

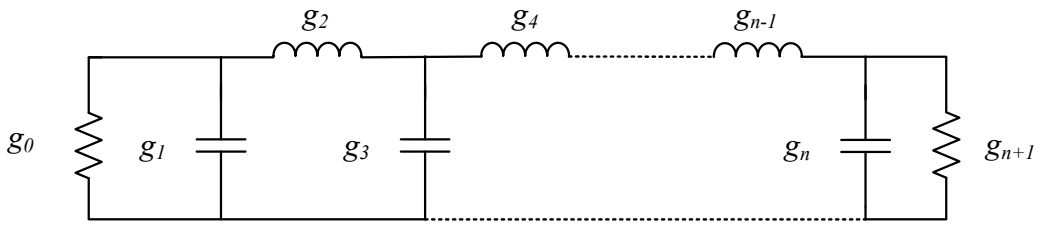

Figure 3.1: General form of the lowpass prototype all-pole filter.

of also lowpass lumped elements normalized both in frequency and impedance. The definition of the filter function is covered in a coming section but it is worth to comment that the synthesis taking place in the lowpass domain is interesting since a synthesized lowpass prototype can be transformed to any position of the bandpass domain to either implement a lowpass, highpass, bandpass or bandstop response, using frequency transformation expressions. In the scope of this thesis, the design of bandpass filters is faced and therefore the bilateral transformation expression for bandpass responses is depicted in a forthcoming section.

The general form of a lowpass prototype ladder filter is shown in figure 3.1, where element values are coefficients g_0 to g_{n+1} that are computed from the lowpass filter function. This schematic depicts the classical shape of a filter that features no transmission zeros, also called an all-pole response. Since no prescribed positions of zero attenuation are present, the element values are general and can be found in tables or the so-called unified design charts. However, since acoustic wave ladder filters are fully canonical, that is featuring as much transmission zeros as resonators, it will be shown that the filter function needs to be specifically computed for each case and that additional elements need to be added to this basic structure.

Notice also that the circuit shown in the figure is a common inline topology. This is that all elements, lumped Ls and Cs in the lowpass domain, are placed one adjacent to the other in a single main line. This is useful for the application of the circuit synthesis approach. In general words, this method implies the evaluation of the polynomials in the $ABCD$ matrix at certain values of the lowpass variable s to extract the values of the lowpass lumped elements. A complete description of this general method can be found in [20].

Now imagine that the objective is not an inline topology but a network whose resonators can be coupled not only with their adjacent but with the rest of the network. To this end, Atia and Williams introduced the concept of the coupling matrix to represent microwave filters in [21]. This representation is made from an admittance point of view and is similar to the concept of adjacency matrix in graph theory. A crucial implication of representing a network in terms of a matrix is that similarity transformations can be applied to it to reconfigure the

topology and achieve new resonator dispositions and couplings that implement the same filter response. In the book by Cameron et al. a general method to compute the coupling matrix of a network is described making use of the eigendecomposition of matrices and the transversal filter topology. In terms of usage, the coupling matrix method is widely used in the design of filters that do not include extracted pole sections. Although out of scope for this thesis, it is worth mentioning that the transformation from transversal to an inline topology made of extracted pole sections does involve non-similar transformations and thus is an open research topic of interest.

In this thesis, since an inline topology where each resonator is responsible for a transmission zero is faced, a specific synthesis technique will be used. This approach is based on the general synthesis procedure introduced by Amari and Macchiarella in [22] and later refined to include cross couplings by Tamiazzo and Macchiarella in [23]. This method is based on extracted pole sections including the concept of non-resonant nodes or NRN. This extent will be revisited in deep in this chapter.

3.2 Lowpass Prototype Filter Functions

The objective of any synthesis procedure is to obtain the circuit elements that implement a transfer function. These functions are defined in the lowpass domain, that is, as functions of the complex variable $s = \sigma + j\omega$, considering a unitary cut-off frequency, i.e. the passband is located in the range $s \in \pm j$ rad/s. As a first step, let us address how can network responses be expressed in terms of lowpass polynomials.

The working principle of a filter mandates that its transfer function has to be defined in terms of how power injected in a network transmits or reflects with respect to the frequency. It is known from microwave theory that the parameters defining transfer and reflection are the reflection $\rho(s)$ and transmission $t(s)$ coefficients, respectively, and in turn, that they are both a function of the normalized input impedance of the network $z(s)$. As the response of the filter is defined in the frequency domain and knowing that a filter is a linear system, $z(s)$ will be a positive real function.

$$z(s) = \frac{n(s)}{d(s)} \tag{3.1}$$

Therefore, the definition of the reflection coefficient is

$$\rho(s) = \frac{z(s) - 1}{z(s) + 1} = \frac{n(s) - d(s)}{n(s) + d(s)} = \frac{F(s)}{E(s)} \tag{3.2}$$

where two characteristic polynomials $P(s)$ and $E(s)$ have been defined. Since

$$|\rho(j\omega)|^2 + |t(j\omega)|^2 = 1 \tag{3.3}$$

it is found that the transmission coefficient contains the third characteristic polynomial $P(s)$.

$$t(s) = \frac{P(s)}{E(s)} \tag{3.4}$$

Therefore, the set of characteristic polynomials that define any filter function are $P(s)$, $F(s)$ and $E(s)$ and must fulfil the following properties:

- $E(s)$ must be an N-th order Hurwitz polynomial to ensure system stability, where N is the order of the filter. This means that all roots of $E(s)$ must be in the left half of the s-plane. This is a consequence of the Routh-Hurwitz criterion mandating that the real part of all roots of $E(s)$ must be negative so that when excited with a driving function, all exponential terms $e^{\alpha t}$ are decreasing (being α the real part of a root of $E(s)$).
- $F(s)$ is an N-th degree polynomial with purely imaginary roots. Reflection zeros (i.e. frequencies at which there is no power reflected) are the roots of $F(s)$.
- $P(s)$ is an n_{tz}-th order polynomial, being n_{tz} the number of transmission zeros, whose roots lie in the imaginary axis, as conjugate pairs in the real axis or as complex quads in the s-plane [20]. The roots of $P(s)$ are the transmission zeros, positions where no signal propagates through the network. In all-pole networks (those that do not feature any transmission zero) $P(s)$ is a constant.

Note that in terms of filter networks, it is desired that all zeros of $F(s)$ are placed inside the passband, and all zeros of $P(s)$ are outside of it.

An important issue to introduce here is the symmetry or asymmetry of responses. Consider that a given transfer function is symmetric around the centre frequency. Therefore, $F(s)$ and $P(s)$ would have purely real coefficients as their zeros would be placed symmetrically on the $j\omega$ axis. This is a condition stated by positive real functions. However, the implementation of asymmetric responses is of interest in many applications, for example acoustic wave filters. Asymmetry means the capability to independently locate upper and lower transmission zeros on a filter.

The traditional lowpass prototype networks, like the one in 3.1, were initially developed to implement symmetric functions but it was known that bandpass domain filters could exhibit asymmetric responses. The challenge was then to find a modification of the lowpass prototypes that would allow the synthesis of asymmetric functions. The mathematical tool devised

for this purpose was the frequency-invariant reactance (FIR) introduced in [24]. These elements act as offsets from the original position of the zeros, either transmission or reflection, and appear in the lowpass prototype circuit as frequency-invariant reactive elements. A complete explanation of this tool and all conditions implied in its development are found in Section 3.10 in [20]. In short, asymmetric responses imply that the starting impedance function is not real positive but only positive, in other words, that has complex coefficients. This implies that $P(s)$ will have complex coefficients, $F(s)$ might have complex coefficients and consequently, $E(s)$ will have complex coefficients as well. The appearance of the FIR elements in the network, will be addressed in an upcoming section.

Back to the matter of defining the filtering function, we have described $\rho(s)$ and $t(s)$. Thus, the filter function can now be expressed in terms of scattering parameters, a more appropriate way for microwave engineers, as $\rho(s) = S_{11}(s)$ and $t(s) = S_{21}(s)$. Considering that a filter is a passive, lossless and reciprocal two-port network, the S-parameter matrix can be defined as follows, being N the order of the network. Variables ε and ε_r are normalization constants used to set the highest-degree coefficient of $P(s)$ and $F(s)$ to one (monic polynomial condition).

$$\boldsymbol{S} = \begin{bmatrix} S_{11}(s) & S_{12}(s) \\ S_{21}(s) & S_{22}(s) \end{bmatrix} = \frac{1}{E(s)} \begin{bmatrix} F(s)/\varepsilon_r & P(s)/\varepsilon \\ P(s)/\varepsilon & -1^N F(s)^*/\varepsilon_r \end{bmatrix} \tag{3.5}$$

Therefore, two conservation of energy equations

$$S_{11}(s)S_{11}(s)^* + S_{21}(s)S_{21}(s)^* = 1 \tag{3.6}$$

$$S_{22}(s)S_{22}(s)^* + S_{12}(s)S_{12}(s)^* = 1 \tag{3.7}$$

and an orthogonality condition

$$S_{11}(s)S_{21}(s)^* + S_{21}(s)S_{22}(s)^* = 0 \tag{3.8}$$

can be derived and from them, two important conclusions are drawn.

From (3.6) and (3.7), one can arrive to what is known as the Feldtkeller equation in (3.9). This equation allows to obtain polynomial $E(s)$ if the other two polynomials $P(s)$ and $F(s)$ and the normalization constants are known. This is the common way to proceed in the computation of the filter function. It is important to mention that operator * refers to the paraconjugation operation in complex-variable polynomials. See further explanation in appendix A.1.

$$E(s)E(s)^* = \frac{F(s)F(s)^*}{\varepsilon_r^2} + \frac{P(s)P(s)^*}{\varepsilon^2} \tag{3.9}$$

Making use of (3.8) in polar coordinates and taking s dependence out of the formulation for simplification, one can obtain an important conclusion of the phases of the scattering

polynomials.

$$|S_{11}|e^{j\theta_{11}} \cdot |S_{21}|e^{-j\theta_{21}} + |S_{21}|e^{j\theta_{21}} \cdot |S_{22}|e^{-j\theta_{22}} = 0$$
$$|S_{11}||S_{21}| \left(e^{j(\theta_{11}-\theta_{21})} + e^{j(\theta_{21}-\theta_{22})}\right) = 0 \tag{3.10}$$

Consequently, this implies that

$$e^{j(\theta_{11}-\theta_{21})} = -e^{j(\theta_{21}-\theta_{22})} \tag{3.11}$$

Considering that the negative sign in the right-hand side of the equation can be replaced by $e^{j(2k\pm1)\pi}$ and examining only the exponents, it yields,

$$\theta_{21} - \frac{\theta_{11}+\theta_{22}}{2} = -\frac{\pi}{2}(2k \pm 1) \tag{3.12}$$

As noted in (3.5), parameters $S_{11}(s)$, $S_{22}(s)$ and $S_{21}(s)$ share the common denominator $E(s)$ and therefore their phases can be understood as being a subtraction of two phases, one from the numerator and one from the denominator (e.g. $\theta_{21}(s) = \theta_{n21}(s) - \theta_d(s)$). This yields an importation rewriting of (3.12), bringing variable s back into play.

$$-\theta_{n21}(s) + \frac{\theta_{n11}(s)+\theta_{n22}(s)}{2} = -\frac{\pi}{2}(2k \pm 1) \tag{3.13}$$

Note that the above equation states that as the right-hand side is an odd multiple of $\pi/2$ and has no dependence in frequency, the difference between the average of phases of S_{11} and S_{22} numerator polynomials and the phase of S_{21} numerator, must be orthogonal at all frequencies. Given this, and following a fine mathematical development of the roots of $F(s)$ detailed in [20], one can reach an interesting equation

$$(N - n_{tz})\frac{\pi}{2}k'\pi = -\frac{\pi}{2}(2k \pm 1) \tag{3.14}$$

being N the order of the filter, n_{tz} the number of transmission zeros and k' and k integers. For the right-hand side to be satisfied, it is mandatory that $N - n_{tz}$ is odd. Therefore, for networks where this quantity is even, for example fully canonical ones where there are N transmission zeros (the ones we are treating), an extra $\pi/2$ radians must be added to the right-hand side of the above equation to fulfil the orthogonality condition. This is adding a shift of $\pi/2$ to $\theta_{n21}(s)$ or equivalently multiplying polynomial $P(s)$ by j. This condition is summarized in table 3.1 extracted from the book by Cameron et al.

Given this conditions, we can now rewrite (3.5) for the two cases.

$$\boldsymbol{S} = \begin{bmatrix} S_{11}(s) & S_{12}(s) \\ S_{21}(s) & S_{22}(s) \end{bmatrix} = \frac{1}{E(s)} \begin{bmatrix} F(s)/\varepsilon_r & jP(s)/\varepsilon \\ jP(s)/\varepsilon & -1^N F(s)^*/\varepsilon_r \end{bmatrix} \qquad \text{for } N - n_{tz} \text{ even} \tag{3.15a}$$

Table 3.1: Satisfaction of the orthogonality condition by multiplying $P(s)$ by j.

N	n_{tz}	$N - n_{tz}$	$jP(s)$
Odd	Odd	Even	Yes
Odd	Even	Odd	No
Even	Odd	Odd	No
Even	Even	Even	Yes

$$\boldsymbol{S} = \begin{bmatrix} S_{11}(s) & S_{12}(s) \\ S_{21}(s) & S_{22}(s) \end{bmatrix} = \frac{1}{E(s)} \begin{bmatrix} F(s)/\varepsilon_r & P(s)/\varepsilon \\ P(s)/\varepsilon & -1^N F(s)^*/\varepsilon_r \end{bmatrix} \qquad \text{for } N - n_{tz} \text{ odd} \tag{3.15b}$$

Having assessed the mathematical conditions that the characteristic polynomials must fulfil and knowing that the procedure will consist in determining $P(s)$ and $F(s)$ and then finding $E(s)$ via the Feldtkeller equation in (3.9), it is interesting to outline the set of functions that might be used to define filters. From the shape point of view, one can define two types of filters: those that include transmission zeros, that is frequencies where signal is not transmitted, and those whose attenuation has a monotonic rise beyond the passband, also called all-pole responses. The transmission zeros of the latter are placed at infinite frequency.

The second classification is made from the polynomial used in the definition of the transfer function. The classical prototype filters are the maximally flat, also called Butterworth filter, that makes use of the polynomials of the same name and shows a maximally flat passband, the elliptic function filters, also called Cauer filters, that show equiripple[1] responses both in the stopband and the passband, and the Chebyshev filters that make use of Chebyshev polynomials and can show equiripple passbands (type I) or equirriple stopbands (type II). There is a strong relation between Cauer and Chebyshev filters as the elliptic might lead to Chebyshev if their in-band or stopband ripples are reduced to zero. A further description and discussion on filtering functions can be found, among others, in the book by Cameron et al. and in the well-known book by Pozar [25].

In terms of the ladder acoustic wave filters, the function that best describes their behaviour is the general class of Chebyshev functions thanks to the introduction of transmission zeros, symmetric and asymmetric characteristics and even and odd degrees [3].

[1] Equalized ripple.

3.2.1 A General Class of the Chebyshev Filter Function

The Generalized Chebyshev filter function has been chosen to obtain the lowpass prototype response of an AW ladder filter. This will be a fully canonical function featuring an equirrippled return loss level. The computation of the function is made via a recursive algorithm but first the Chebyshev function must be described.

3.2.1.1 Computation of ε and ε_r

The paper of constants ε and ε_r is normalizing the characteristic polynomials to be monic and so, in order to obtain $E(s)$ from the other two polynomials, they must be previously found. To do so, note in (3.5) that ε can be obtained by evaluating parameter S_{21} at a frequency where its value is know. In the case of Chebyshev filters, the equirriple return loss (RL) level is prescribed at the border of the passband (i.e. $s = \pm j$, equivalently $\Omega = \pm 1$)[2].

$$\varepsilon = \frac{1}{\sqrt{1 - 10^{-RL/10}}} \left| \frac{P(s)}{E(s)} \right|_{s=\pm j} \tag{3.16}$$

However, $E(s)$ is not know yet. Then, by looking at the definition of the S-parameters, this equation might be transformed to

$$\frac{\varepsilon}{\varepsilon_r} = \frac{1}{\sqrt{10^{-RL/10} - 1}} \left| \frac{P(s)}{F(s)} \right|_{s=\pm j} \tag{3.17}$$

Now we should find the value of ε_r, that can be assessed from parameter S_{11}. Note that for a network featuring transmission zeros at infinity (i.e. $N - n_{tz} > 0$), it is known that $S_{21}(s = \pm j\infty) = 0$ and so, $S_{11}(s = \pm j\infty) = 1$ because of the conservation of energy condition (3.6). As polynomials must be monic, it is clear that $\varepsilon_r = 1$. However, for a fully canonical network, the evaluation of transmission at infinite frequency has a finite value and therefore, another time evaluating the conservation of energy at $s = \pm j\infty$ it can be derived that,

$$\varepsilon_r = \frac{\varepsilon}{\sqrt{\varepsilon^2 - 1}} \tag{3.18}$$

In conclusion, for AW ladder filters, that are fully canonical, these two constants are defined by (3.17) and (3.18).

[2]From this point onwards, we will move from the s-plane to the Ω-plane (i.e. $s = j\Omega$, the real lowpass frequency variable) for simplicity. This lowpass frequency is referred as Ω not to mess with the bandpass angular frequency, commonly termed, ω.

3.2.1.2 Polynomial Synthesis of Chebyshev Functions

With the objective of computing the Chebyshev filter function characteristic polynomials, the formulation starts by expressing parameter $S_{21}(\Omega)$ in terms of the filtering function, let it be $C_N(\Omega)$, and a normalization constant k used only for mathematical completeness to consider that in general Chebyshev polynomials ($C_N(\Omega)$) are not monic.

$$|S_{21}(\Omega)|^2 = \frac{1}{1+\left|\frac{\varepsilon}{\varepsilon_r}kC_N(\Omega)\right|^2} = \frac{1}{1+\left|\frac{\varepsilon}{\varepsilon_r}\frac{F(\Omega)}{P(\Omega)}\right|^2} \tag{3.19}$$

The poles and zeros of $C_N(\Omega)$ are the transmission and reflection zeros respectively, that is, the roots of $P(\Omega)$ and $F(\Omega)$. Function $C_N(\Omega)$ is the expression of the Chebyshev polynomials of the first kind (namely $T_n(x)$) where x is a function of frequency, $x_n(\Omega)$, instead of a simple variable[3].

$$C_N(\Omega) = \cosh\left[\sum_{n=1}^{N} cosh^{-1}(x_n(\Omega))\right] \tag{3.21}$$

In turn, function $x_n(\Omega)$ must fulfil some properties to describe a Chebyshev function:

- $x_n(\Omega_n) = \pm\infty$ at Ω_n being a transmission zero or infinity.
- In-band (i.e. $-1 \leq \Omega \leq 1$), $1 \geq x_n(\Omega) \geq -1$.
- At $\Omega = \pm 1$, namely the passband edges, $x_n(\Omega) = \pm 1$.

By developing the three conditions above, the function is found to be

$$x_n(\Omega) = \frac{\Omega - \frac{1}{\Omega_n}}{1 - \frac{\Omega}{\Omega_n}} \tag{3.22}$$

Figure 3.2 shows an example of the function $x_n(\Omega)$ for a transmission zero at 1.4. The vertical lines in the plot mark the edges of the passband.

Now that the mathematical description of the filtering function is complete. The first step is to compute polynomial $P(\Omega)$ since it is known that its roots are the transmission zeros and they are prescribed by the designer. Thus, given a set of N transmission zeros this

[3]Note that the interval of $\operatorname{arccosh}(x)$ is $[1, \infty)$. Therefore for a correct analysis of $C_N(\Omega)$, we might make use of the identity $\cosh\theta = \cos j\theta$ [20] yielding the following expression for $\Omega \leq 1$

$$C_N(\Omega) = \cos\left[\sum_{n=1}^{N} cos^{-1}(x_n(\Omega))\right] \tag{3.20}$$

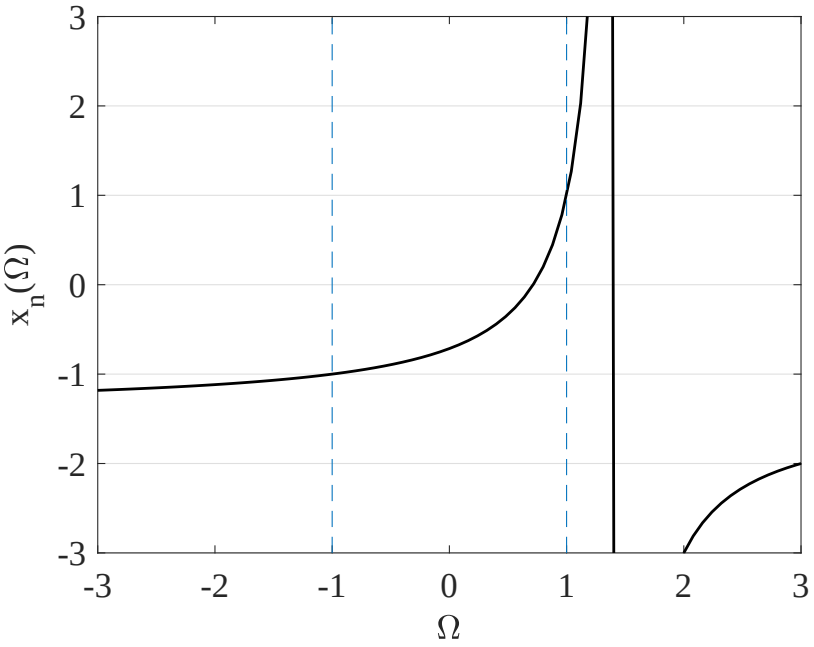

Figure 3.2: Function $x_n(\Omega)$ for $\Omega_n = 1.4$

polynomial can be automatically constructed as follows, considering that for networks with no transmission zeros, $P(\Omega) = 1$.

$$P(\Omega) = \prod_{n=1}^{N} (\Omega - \Omega_n) \tag{3.23}$$

The process to find $F(\Omega)$ is slightly more complex as it involves a recursive computation of N steps. The detailed development of this solution is presented by Cameron et al. in section 6.3 of their book [20]. Starting from (3.21), replacing cosh x by its logarithmic identity and after some cumbersome grouping, the expression can be broken down to a multiplication of sums and subtractions of two terms:

$$c_n = \left(\Omega - \frac{1}{\Omega_n}\right) \quad \text{and} \quad d_n = \Omega' \sqrt{1 - \frac{1}{\Omega_n^2}} \tag{3.24}$$

The recursive technique makes use of two auxiliary polynomials $U(\Omega)$ and $V(\Omega)$ during N iterations. At each iteration, the new value of $U_i(\Omega)$ and $V_i(\Omega)$ is computed from $U_{i-1}(\Omega)$ and $V_{i-1}(\Omega)$, and the i-th root of $P(\Omega)$, namely Ω_i. If there are less than N transmission zeros, the $N - n_{tz}$ extra roots are $\Omega_i = \infty$.

The first iteration, $i = 1$, is started as follows

$$U_1(\Omega) = c_1 \quad \text{and} \quad V_1(\Omega) = d_1 \tag{3.25}$$

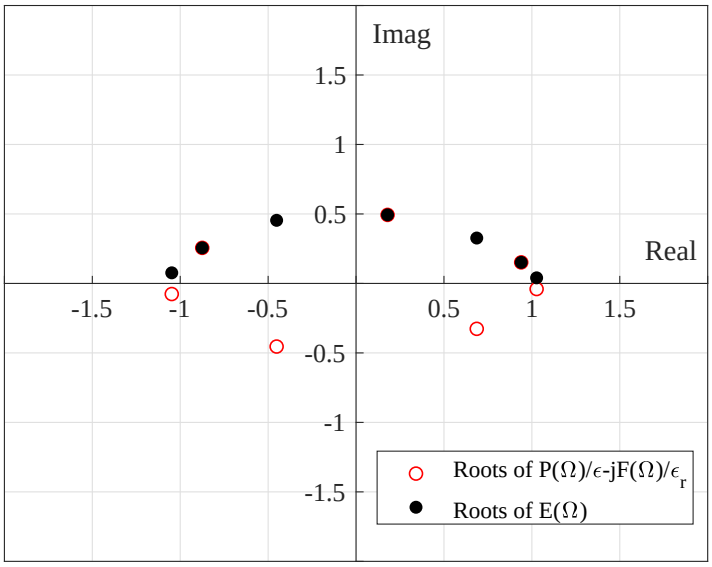

Figure 3.3: Comparison of the roots of $P(\Omega)/\varepsilon - jF(\Omega)/\varepsilon_r$ and $E(\Omega)$ in the ω-plane.

from $i = 2$ to $i = N$, the polynomials are computed as

$$U_i(\Omega) = c_i U_{i-1} + d_i V_{i-1}(\Omega) \tag{3.26a}$$

$$V_i(\Omega) = c_i V_{i-1} + d_i U_{i-1}(\Omega) \tag{3.26b}$$

After N iterations, polynomial $U(\Omega)$ has the roots of the numerator of $C_N(\Omega)$, or what is the same, the roots of $F(\Omega)$. Up to this moment $P(\Omega)$, $F(\Omega)$ and their normalization constants ε and ε_r have been found. Now, the Feldtkeller equation in (3.9) can be applied to obtain $E(\Omega)$ by building polynomial $P(\Omega)/\varepsilon - jF(\Omega)/\varepsilon_r$. It has been stated in a previous section that polynomial $E(\Omega)$ must be Hurwitz, what means that the real part of all its roots must be in the left-hand side of the complex s-plane. This is equivalent to the upper-half of the Ω plane. Therefore, by rooting the constructed polynomial in Ω and conjugating each root lying in the lower-half of the Ω plane, the roots of $E(\Omega)$ are found.

For illustration purposes let us a consider a 7-th order network with a set of transmission zeros $\Omega_{tz} = [1.2, -2.5,\ 1.7, -1.6,\ 3.3, -2.1,\ 2.1]$ and return loss level of $RL = 18$ dB. By following all steps described above, that can be easily implemented using Matlab, the characteristic polynomials are obtained and summarized in table 3.2. Figure 3.3 shows the roots of $P(\Omega)/\varepsilon - jF(\Omega)/\varepsilon_r$ and the final roots of the Hurwitz polynomial $E(\Omega)$. Polynomial $P(\Omega)$ already includes the multiplication by j because of N being odd. The Generalized Chebyshev function response can be plotted in terms of S-parameters using (3.15b) and is depicted in figure 3.4.

Table 3.2: Generalized Chebyshev polynomial synthesis example of a 7-th order network.

s^i for $i =$	$P(s)$	$F(s)$	$E(s)$
7	$j1.0000$	1.0000	1.0000
6	2.1000	$-j0.4574$	$1.7981 - j0.4574$
5	$j14.2200$	1.8237	$3.4402 - j0.8352$
4	25.3300	$-j0.7399$	$3.6135 - j1.5026$
3	$j62.1009$	0.9678	$3.2108 - j1.5158$
2	97.7923	$-j0.3137$	$1.8853 - j1.2140$
1	$j83.0791$	0.1328	$0.7729 - j0.6106$
0	118.7500	$-j0.0224$	$0.1579 - j0.1800$
	$\varepsilon = 498.1367$	$\varepsilon_r = 1.0$	

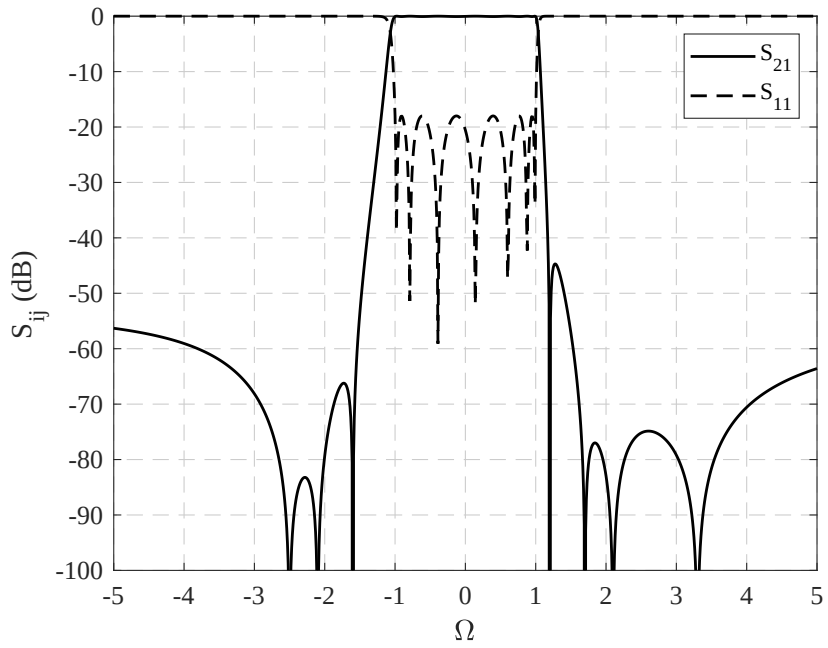

Figure 3.4: Lowpass prototype response of the 7-th order example network.

3.3 Lowpass Prototype of the Acoustic Wave Resonator

The lowpass filter function to be synthesized has been defined in the previous section and it has been stated previously that the synthesis takes places in the lowpass domain (s or Ω frequency variable) and the computed elements are later transformed to the bandpass domain (f or ω frequency variable) and scaled in impedance. Therefore, it is important to find a model

to represent the resonator in the lowpass domain, and to do so, the well-known bilateral frequency transformation function needs to be assessed (3.27),

$$\Omega = \frac{\omega_0}{\omega_2 - \omega_1}\left(\frac{\omega}{\omega_0} - \frac{\omega_0}{\omega}\right) \tag{3.27}$$

being ω the bandpass angular frequency variable, ω_1 and ω_2 the passband edges and ω_0 the centre frequency of the passband that is computed as the geometric mean of the edges. Commonly, the term $\omega_0/(\omega_2 - \omega_1)$ is grouped under variable α, namely the inverse of the relative bandwidth.

To illustrate the use of this function, let us observe the case of an unscaled lowpass lumped inductor of value L. It is clear that the impedance of this element is $Z(\Omega) = j\Omega L$. Apply now (3.27) to this impedance expression.

$$Z(\omega) = \frac{j\alpha\omega L}{\omega_0} + \frac{\alpha\omega_0 L}{j\omega} \tag{3.28}$$

This expression is equivalent to the impedance of a series LC that is resonant at ω_0, whose elements are

$$L_r = \frac{\alpha L}{\omega_0} \qquad \text{and} \qquad C_r = \frac{1}{\alpha\omega_0 L} \tag{3.29}$$

Similarly, it can be proven that a lowpass lumped capacitor will transform to a shunt LC tank.

The important conclusion of this is that frequency dependent lowpass values transform to resonators whose resonance is at the centre frequency of the filter. This is why simple lowpass prototype circuits made of lumped inductors and capacitors can only implement symmetrical filter functions, and is also the justification of the need of FIR elements introduced at the beginning of section 3.2.

Imagine that we want to represent, in the lowpass domain, a resonator whose resonance is placed at an arbitrary position in-band but not at its centre. We have seen that classical lumped elements become resonators at ω_0 and therefore we seek a way to implement a frequency detuning of the resonator in question. The tool proposed by Baum [24] in 1957 was a hypothetical element of reactive nature whose reactance does not depend in frequency, in other words, the FIR. Due to the frequency independence, their transformation to the bandpass domain is only an impedance scaling and hence, are implemented as single elements. In terms of notation, FIR elements are commonly referred to as X or B.

The main limitation of this tool is that it is only accurate for narrow bandwidths because of the frequency independence assumption. FIR elements present in the lowpass prototype network must be implemented by means of reactive elements in the bandpass domain, and as stated by Ronald M. Foster in his theorem [26], the reactance of any passive element always

increases monotonically. Therefore, it is only possible to approximate a constant reactance with a real reactive element in a narrow bandwidth, achieving equality only at a single point in frequency. As seen in chapter 2, the bandwidth of ladder filters made of acoustic resonators is limited by the electromechanical coupling coefficient. This yields relatively narrow desired bandwidths and makes FIRs suitable to appear in the representation of acoustic wave filters in the lowpass domain.

The further we get from the frequency of equal reactances, the more deviation between the ideal lowpass FIR and the real frequency-dependent element that implements it. Thus, it can be seen that if FIRs are present, the transformation in (3.27) will be perfectly accurate at the point of evaluation but its accuracy will decrease the further we move from that frequency. The selection of this frequency where equality of reactances is imposed is essential as it will define which part of the lowpass filter response is mapped exactly in the transformation to the bandpass domain. The stringent specifications of mobile phone bands mandate that the in-band response (i.e. insertion losses and equirriple, among others) is the most important mask of the device, while the exact position of transmission zeros with respect to the lowpass function can be slightly more relaxed[4]. Therefore, the frequency evaluation point of the FIR elements is defined as the centre frequency of the passband, ω_0.

Back to the model of an acoustic resonator, the bandpass model that we aim to reach after transformation is not a common LC tank but the BVD model. As presented in previous chapters, the motional branch of the BVD is composed by an LC series resonator. Then, it is clear that this branch will be a lowpass inductive element. However, we know that the series resonance of an AW resonator is not at the centre frequency of the filter rather than at a frequency defined by the thickness of the resonator in BAW or the IDT distance in SAW. A FIR element in series to the inductive element is therefore needed to tune this resonance. In parallel, quite literally, the static branch of the BVD does not feature any resonance and thus, the static capacitance C_0 must be modelled as a FIR element in the lowpass domain. Hence, the resulting lowpass model for an acoustic resonator is depicted in figure 3.5.

The input impedance of this model can be computed as

$$Z_{in}(\Omega) = \frac{jX_0\left(\Omega L_m + Xm\right)}{\Omega L_m + X_m + X_0} \tag{3.30}$$

In turn, the input impedance of the BVD is known in (2.4). To find the relation between the bandpass and the lowpass elements, the impedance of the static and motional branches must be separately equated at the centre frequency of the filter ω_0.

[4]This means that a one-to-one match between lowpass and bandpass responses is not expected at the exact position of transmission zeros.

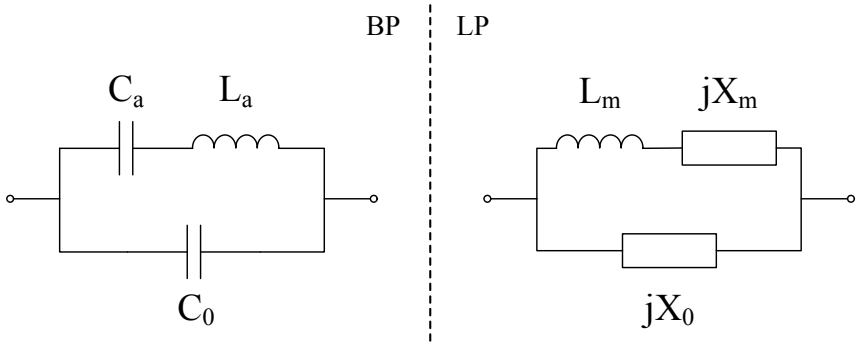

Figure 3.5: Bandpass and lowpass model of the Butterworth - Van Dyke circuit.

In the case of the static branch[5], being Z_0 the reference impedance needed to scale the normalized lowpass value, it results

$$Z_s(\Omega)Z_0 = Z_s(\omega)$$
$$jX_0Z_0 = \left.\frac{1}{j\omega C_0}\right|_{\omega=\omega_0}$$

yielding the static capacitance C_0 to be

$$C_0 = -\frac{1}{\omega_0 Z_0 X_0} \tag{3.31}$$

In the case of the motional branch we shall follow the same procedure, but two unknowns are present, L_a and C_a.

$$Z_m(\Omega)Z_0 = Z_m(\omega)$$
$$j(X_m + \Omega L_m)Z_0 = j\left(\omega L_a - \frac{1}{\omega C_a}\right)$$
$$\left[X_m + \alpha L_m\left(\frac{\omega}{\omega_0} - \frac{\omega_0}{\omega}\right)\right]Z_0 = \left(\omega L_a - \frac{1}{\omega C_a}\right) \tag{3.32}$$

Differentiating (3.32) with respect to ω we obtain the second equation. Then, we can evaluate at $\omega = \omega_0$ and isolate the two bandpass elements.

$$L_a = \frac{Z_0}{2}\left(\frac{2\alpha L_m + X_m}{\omega_0}\right) \tag{3.33}$$

$$C_a = \frac{2}{Z_0}\frac{1}{\omega_0(2\alpha L_m - X_m)} \tag{3.34}$$

3.3.1 Nodal Representation of the Lowpass Acoustic Wave Resonator

Based on the coupling matrix vision previously introduced and on the fact that, due to the dual-network theorem, ladder lowpass prototypes can be expressed as prototypes made of

[5]Here we use Z_s from *static* not to mess with the reference impedance Z_0.

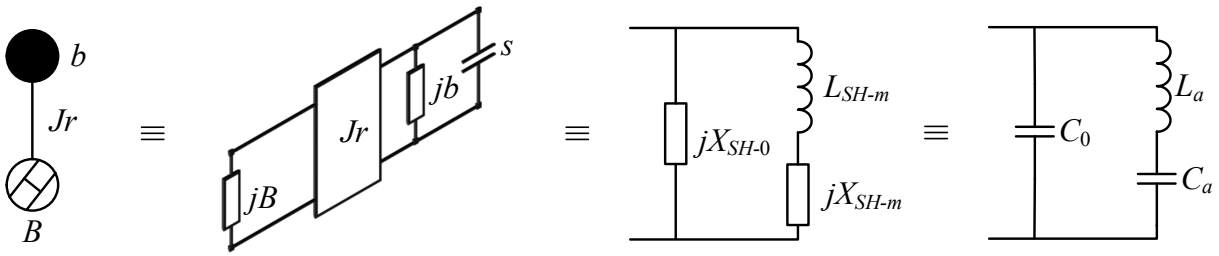

Figure 3.6: Lowpass representation of a dangling resonator in nodal and circuital views, and its relation with the model of a shunt acoustic resonator.

shunt elements placed between admittance inverters, a lowpass network can be interpreted from the nodal point of view: a network made of nodes, resonant or not, that are coupled using inverters. This depiction of the network is of interest as it simplifies the guidance through the synthesis procedure.

Amari and Macchiarella introduced in [22] that an extracted pole section, namely a resonator responsible for the introduction of a transmission zero (TZ), can be represented in the lowpass domain by a unitary capacitor connected in parallel to a constant reactance (FIR) of value $jb_i = j\Omega_i$, being Ω_i the frequency of the zero. This resonator is said to be dangling from the main line of the topology by means of an admittance inverter J_r and connected to a non-resonant node or NRN, that is, a node connected to ground by means of a FIR, B. The concept of NRNs, the application of FIRs to the nodal representation, was introduced by Amari in [27]. Figure 3.6 depicts a dangling resonator[6].

Let us analyse the input admittance[7] of the dangling resonator.

$$Y_{in}(s) = jB + \frac{J_r^2}{s + jb} \tag{3.35}$$

This expression has a behaviour equivalent to that shown by the BVD model. At $s = -jb$ the admittance becomes infinite, placing a transmission zero at $\Omega = -b$, and similarly there is a position where the admittance is zero. The position of the TZ is only dependent on the value of FIR b, that can either be positive or negative. This feature of the dangling resonator defines it as the basic building block for the synthesis of extracted pole inline filters.

The relations between the nodal elements B, b and J_r with the elements of a shunt lowpass

[6]From this point onwards, terms NRN and FIR might be used to refer to the same concept, as the non-resonant node is a FIR element.

[7]The nodal representation here explained and introduced in the synthesis by Amari and Machiarella, is faced from the admittance point of view. That is why unitary shunt capacitors are used as resonant elements.

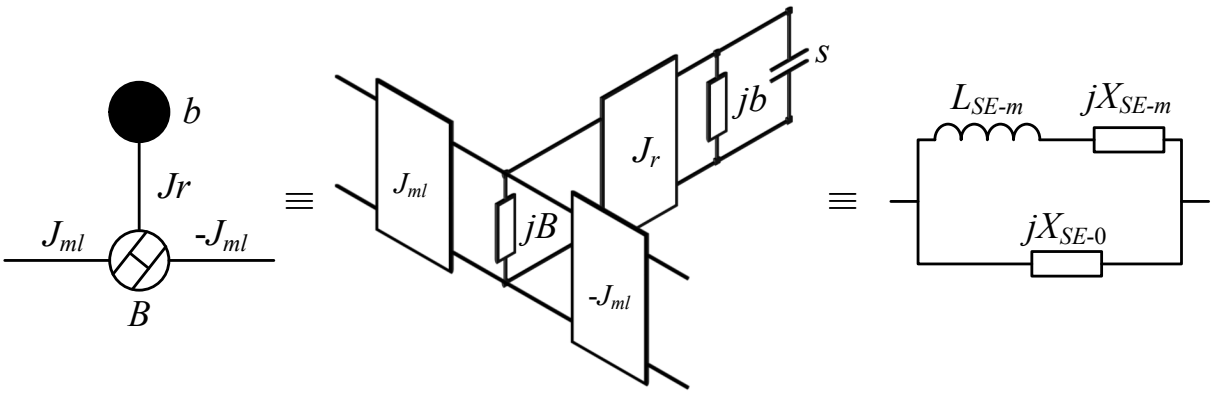

Figure 3.7: Series acoustic wave resonator in lowpass nodal, circuital and BVD views.

BVD, as shown in figure 3.6, are developed by Giménez in [28, 3] as

$$X_{0-SH} = -\frac{1}{B} \tag{3.36a}$$

$$L_{m-SH} = \frac{1}{J_r^2} \tag{3.36b}$$

$$X_{m-SH} = \frac{b}{J_r^2} \tag{3.36c}$$

We have already seen that in the ladder filter, transmission zeros below the passband, corresponding to negative zeros in the lowpass domain, are implemented by shunt acoustic resonators. On the other hand, positive lowpass transmission zeros are implemented by series acoustic resonators. Since a dangling resonator will, by definition, transform to a resonator in shunt configuration with respect to the main line of the filter, it will be used to represent shunt acoustic resonators. More specifically, shunt acoustic resonators whose series resonance is directly related to the FIR b.

At this point, to face the implementation of positive transmission zeros we will another time consider the dual-network theorem to see that a series resonator can be obtained if a dangling resonator is placed between admittance inverters of opposite sign, i.e. two admittance inverters are connected to the FIR B. These inverters are noted as J_{ml}, as they are part of the main line of the filter, and the opposition of signs is needed not to alter the phase characteristics of the dangling resonator.

The lowpass BVD elements of the series resonator are now defined as

$$X_{0-SE} = \frac{B}{J_{ml}^2} \tag{3.37a}$$

$$L_{m-SE} = \frac{B^2}{J_r^2 J_{ml}^2} \tag{3.37b}$$

$$X_{m-SE} = \frac{B}{J_{ml}^2}\left(b\frac{B}{J_r^2} - 1\right) \tag{3.37c}$$

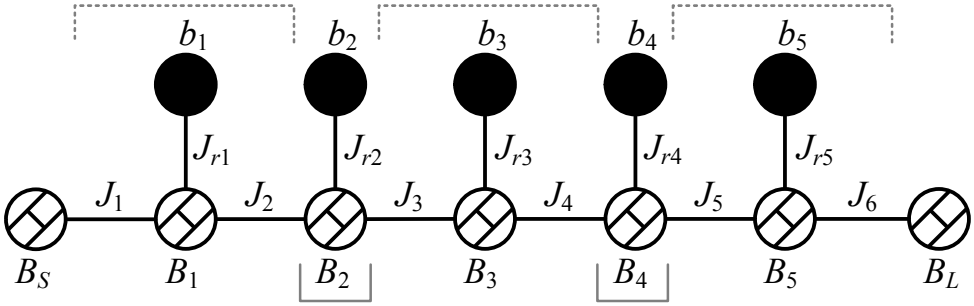

Figure 3.8: Nodal representation of a 5-th network starting in series resonator. Underlined resonators are shunt, overlined resonators are series.

Having defined the two resonator configurations present in the ladder topology, figure 3.8 presents the nodal representation of an entire filter network on which the synthesis might be performed. This schematic might be, for example, the lowpass equivalent of the acoustic ladder filter shown in figure 2.6. Observe that the proposed network starts with a series resonator.

The source node of the network is a FIR of name B_S. Similarly, there is a load FIR B_L. The need of these FIRs in acoustic wave filter networks will be discussed in the next subsection and is of importance in the subject of this thesis. Note that these source and load FIR elements will transform to shunt input/output reactive elements, either capacitors or inductors depending on the sign of $B_{S/L}$. These elements have been presented as necessary in ladder topologies in 2.3.1.

Before proceeding with the synthesis, two interesting aspects shall be commented. The first concerns a condition of fully canonical networks presented in [20]: a fully canonical network features an inherent direct source-to-load coupling. This might not be seen directly in the proposed nodal scheme, but it is present. Thanks to the dangling resonator structure a direct reactive path between source and load is achieved across the main line and the NRNs. Secondly, by inspecting nodal-to-circuital equations (3.37) and (3.36), it can be inferred that to ensure that the static branch element is capacitive, synthesized FIR B must be negative for series resonators and positive for shunt resonators. This will take an important paper in the treatment of shunt-starting networks.

3.3.2 The Role of Source and Load FIRs

The extracted pole nature of the network presented involves proper consideration of the input phase of the network. This input phase is the phase of parameter $S_{11}(s)$.

Imagine that the first node of a network is a resonant node, i.e. a black ball in nodal

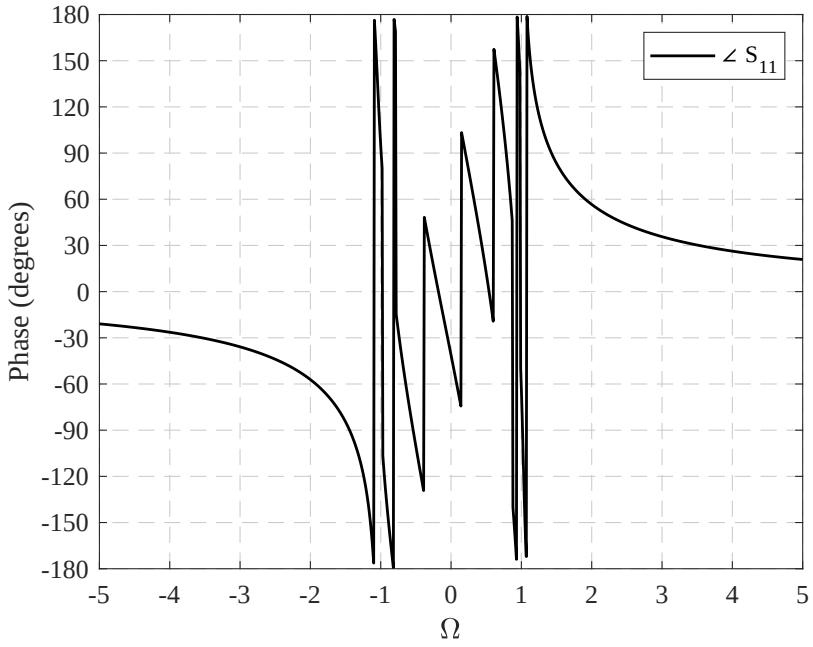

Figure 3.9: Intrinsic input phase of the 7-th order Generalized Chebyshev filter function of figure 3.4.

representation, placed in the main line. We know that a resonant node will transform to a common LC circuit, and by definition, an inline network featuring a pure LC tank will have at least one transmission zero at infinity. This means that at infinite frequency, using (3.5), $S_{11}(s = j\infty) = 1$ since $E(s)$ and $F(s)$ are monic and $\varepsilon_r = 1$. However, for a fully canonical network, there are no zeros at infinity but at finite frequencies. Let us evaluate $S_{11}(s = j\Omega_1)$, the first TZ. The result is that $S_{11}(j\Omega_1) \in \mathbb{C}$. We would expect it to be 1, but it is a complex number of unitary absolute value and a remaining phase, namely $|S_{11}(j\Omega_1)| = 1$ and $\angle S_{11}(j\Omega_1) \neq 0$. This result is perfectly comprehensible by inspecting the input phase response of the Generalized Chebyshev function depicted in figure 3.9. This function is the 7-th order example computed before. At the frequency of the first transmission zero, $\Omega = 1.2$, there is a remaining phase of 125.88 degrees. Imagine that the network in figure 3.8 started directly with J_1 and our intention is to extract the elements of the first dangling resonator. If we evaluate at the first transmission zero, b_1 would act as a short circuit and B_1 in parallel with a short circuit would be neglected. However, we would be facing a resonator at resonance that should have an input phase of 0^o but we know from the filter function that there is a remaining phase. This mandates that this remaining phase has had to be accommodated before facing the first dangling resonator for a proper implementation of the Generalized Chebyshev filter function in the topology. Accommodating this phase imposes that a source FIR B_S must be present at the input of the network as a phase matching element. The same applies if the network

is faced from load to source, thus imposing load element B_L. Following this reasoning, note that in general, although FIR B_1 is part of the first resonator and will transform to the first acoustic resonator, the element itself is acting as a phase matching element for the following dangling section.

Another important implication derives from this approach. Considering that a complex number can be shifted an arbitrary phase without being affected in its absolute value, see that we can define parameter $S_{11}(s)$ as in (3.38) without affecting its magnitude response, because θ_{add} is a real number in radians.

$$S_{11}(s) = \frac{F(s)/\varepsilon_r}{E(s)} e^{j\theta_{add}} \tag{3.38}$$

This additional phase term has a very important role in the design of acoustic filters. As a first example, consider that we want to design a stand-alone filter (stand-alone means that is not part of a duplexer or multiplexer). From the reasoning above it is seen that we would need input and output reactive elements in the topology for its proper functioning, because of the intrinsic phase of the Chebyshev filter function. However, notice that it is possible to find an additional phase that ensures that the input phase to the first resonator is 0 degrees, in other words, that $\angle S_{11}(j\Omega_1) = 0$. This phase can be computed as in (3.39).

$$\theta_{add} = -\arg\left(\frac{F(s)/\varepsilon_r}{E(s)}\bigg|_{s=j\Omega_1} \right) \tag{3.39}$$

In terms of applying the phase shift to the filter function, it is commonly done in polynomial $F(s)$, directly as $F'(s) = F(s)e^{j\theta_{add}}$. If we apply the additional phase we just computed, as the phase at the first TZ is zero, the source FIR element B_S is no longer necessary and in the bandpass domain it would result in an acoustic wave ladder filter that does not need an input reactive element.

Note that by tuning the phase on $F(s)$, both S_{11} and S_{22} are modified anti-symmetrically, following the condition stated in (3.13). Separate tuning of the phase implies the construction of the so-called asymmetric polynomials, $F_{11}(s)$ and $F_{22}(s)$ and a careful selection of the input and output phases. This is a hot research topic in acoustic wave filter synthesis and important advances have been made by other researchers at the Antenna and Microwave Group at UAB.

On the other hand, input phase tailoring is also of paramount importance in the synthesis of duplexers and multiplexers, and this extent will be explained in following sections after the synthesis procedure has been introduced.

3.4 Synthesis Procedure

The synthesis procedure implemented in this thesis is the one proposed by Tamiazzo and Macchiarella in [23]. This procedure allows to synthesize networks including resonant (RN) and non-resonant (NRN) nodes not only of pure inline but also of cross-coupled topologies. That is, networks with NRNs that might be arbitrarily coupled to each other. Up to the dissemination of this paper, this extent had not been possible and the synthesis of extracted pole sections was only considered for inline topologies. In the scope of this thesis, the cross-coupling feature of the procedure will not be exploited, but has already been used by Triano in [29] to explore the effects of electromagnetic couplings through the packaging of acoustic wave filters.

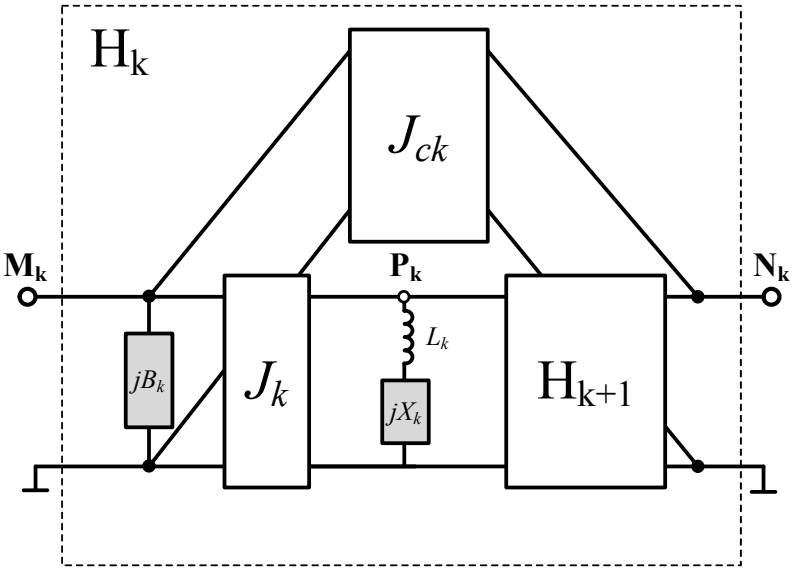

Figure 3.10: Subnetwork considered at the k-th step of the recursive synthesis procedure.

This synthesis method is a recursive process of $N+1$ steps, moving along the topology. The procedure can be applied from source to load, load to source or alternating source and load extractions, and to conduct it throughout the network during the extraction of parameters, Tamiazzo proposes three indices, M_k, N_k and P_k, to numerate nodes. In this thesis, the process is used source to load, but for high order filters, numerical stability issues arise and alternating source and load extractions become a better choice. The aforementioned indices can be observed in figure 3.10. This figure depicts the subnetwork that is considered at each step of the synthesis. H_k is the subnetwork considered at the k-th step, and H_{k+1} is the remaining network for the next step. J_k is the main line admittance inverter whose value is fixed to unity, jB_k is the FIR element of the main line NRN (B_i in the nodal network in figure 3.8), J_{ck} is the cross-coupling between nodes M_k and N_k, and inductance L_k and FIR jX_k

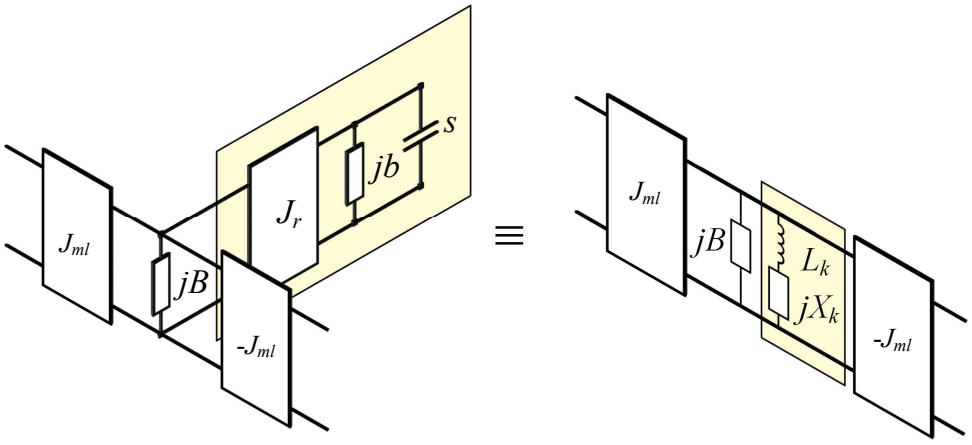

Figure 3.11: Equivalence between dangling resonator and subnetwork section L_k, X_k.

compose the dangling resonator branch, made of J_r, c and b as depicted in figure 3.11.

The equations relating the elements of the dangling branch are the following:

$$L_k = \frac{1}{J_r^2} \qquad \text{and} \qquad X_k = \frac{b}{J_r^2} \tag{3.40}$$

These equations are equal to those presented in (3.36) for a shunt AW resonator, but note that the subnetwork figure defines an important characteristic of the synthesis procedure that has already been introduced in section 3.3.2. In figure 3.10, element jB_k (the NRN) and L_k and jX_k do not belong to the same resonator. As the NRN of a dangling resonator acts as a phase matching element to the next dangling section, the extraction of this elements is computed at the same step. In simpler words, in figure 3.8, B_S, J_1, J_{r1} and b_1 are extracted at step $k = 1$. At the k-th step, they would be B_{k-1}, J_k, J_{rk} and b_k.

From a mathematical perspective the network is represented using the *ABCD* matrix, as in the following expression:

$$[ABCD] = \frac{1}{jP(s)/\varepsilon} \begin{bmatrix} A(s) & B(s) \\ C(s) & D(s) \end{bmatrix} \tag{3.41}$$

where polynomials $A(s)$, $B(s)$, $C(s)$ and $D(s)$ can be expressed as a function of the polynomial coefficients of $F(s)/\varepsilon_r$ and $E(s)$ as presented in appendix A.2.[8] Once the *ABCD* polynomials have been computed the extraction of elements can start. This method allows to extract either extracted pole sections at a root of $P(s)$ (TZs imposed in the filter function), a resonant node at infinity, an extracted pole section at an arbitrary frequency $j\Omega_k$ using cross-couplings or a dual transmission zero [28]. In this case, the explanation will focus on the extraction of roots of $P(s)$ to compose fully canonical networks without cross-couplings.

[8]The usage of B_k as the nomenclature for the FIR element at the k-th iteration might lead to confusion with polynomial $B(s)$. Hence, frequency dependence on s will always be depicted to avoid confusion.

Following the scheme depicted in figure 3.10, the first thing to extract in a synthesis step is the cross-coupling J_{ck}. Although no cross-couplings are considered, and all extractions are performed at roots of $P(s)$, this step is included for completeness. It can be extracted as follows:

$$J_{ck} = -\frac{P_k(j\Omega_k)}{B_k(j\Omega_k)} \tag{3.42}$$

It is clear that as long as the TZ Ω_k is a root of $P(s)$, the value of $J_{ck} = 0$. After this extraction, the remaining network is noted as H'_k and thus $[ABCD]'_k$. The following extraction is the FIR element B_k that prepares the extraction of the actual transmission zero. It is computed as

$$B_k = \frac{D'_k(j\Omega_k)}{B'_k(j\Omega_k)} \tag{3.43}$$

After extracting B_k, the remaining $[ABCD]$ polynomials must be updated as

$$[ABCD]''_k = \frac{1}{jP''_k(s)} \begin{bmatrix} A''_k(s) & B''_k(s) \\ C''_k(s) & D''_k(s) \end{bmatrix} = \frac{1}{jP'_k(s)} \begin{bmatrix} A'_k(s) & B'_k(s) \\ C'_k(s) - B_k A'_k(s) & D'_k(s) - B_k B'_k(s) \end{bmatrix} \tag{3.44}$$

The next extracted element is the admittance inverter J_k. Its value has been fixed to unity, for reasons that will be introduced after the synthesis, and therefore the polynomials should also be updated to $[ABCD]'''_k$, as follows

$$[ABCD]'''_k = \frac{1}{jP'''_k(s)} \begin{bmatrix} A'''_k(s) & B'''_k(s) \\ C'''_k(s) & D'''_k(s) \end{bmatrix} = \frac{1}{jP''_k(s)} \begin{bmatrix} -jC''_k(s) & -jD''_k(s) \\ -jA''_k(s) & -jB''_k(s) \end{bmatrix} \tag{3.45}$$

As a last extraction at this k-th synthesis step, inductance L_k in series with the FIR jX_k must be extracted. In figure 3.11 and (3.40) the relation between these elements and the dangling resonator parameters has been presented. It is already known that this dangling section introduces a TZ at $\Omega_k = -b_k$ therefore it is clear that $b_k = -\Omega_k$. Let us look at the input admittance evaluated at this root.

$$Y_{in}(j\Omega_k) = \frac{D'''_k(j\Omega_k)}{B'''_k(j\Omega_k)} = \left.\frac{J_{rk}^2}{s - j\Omega_k}\right|_{s=j\Omega_k} \tag{3.46}$$

It has the typical partial fraction expansion form: a residue divided by a pole. Therefore, we can make use of the Heaviside cover-up method to obtain the residue as

$$J_{rk}^2 = \left.\frac{D'''_k(s)(s - j\Omega_k)}{B'''_k(s)}\right|_{s=j\Omega_k} = \frac{D'''_k(j\Omega_k)}{\tilde{B}_k(j\Omega_k)} \tag{3.47}$$

After this extraction all polynomials must be updated to conform the $[ABCD]$ matrix of the remaining subnetwork H_{k+1}, as follows

$$[ABCD]_{k+1} = \frac{1}{j\tilde{P}_k(s)} \begin{bmatrix} \tilde{A}_k(s) & \tilde{B}_k(s) \\ \tilde{C}_k(s) & \tilde{D}_k(s) \end{bmatrix} = \frac{(s - j\Omega_k)}{jP'''_k(s)} \begin{bmatrix} \dfrac{A'''_k(s)}{(s - j\Omega_k)} & \dfrac{B'''_k(s)}{(s - j\Omega_k)} \\ \dfrac{C'''_k(s) - J_{rk}^2 \tilde{A}_k(s)}{(s - j\Omega_k)} & \dfrac{D'''_k(s) - J_{rk}^2 \tilde{B}_k(s)}{(s - j\Omega_k)} \end{bmatrix} \tag{3.48}$$

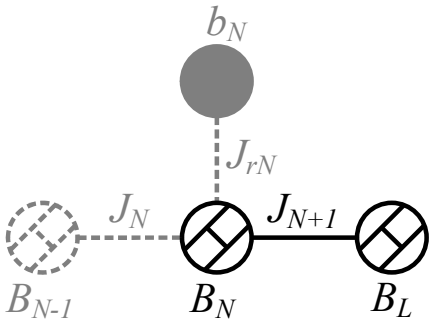

Figure 3.12: Nodal elements faced in the last iteration of the synthesis. In grey are those elements that have already been extracted.

With this, a synthesis step is completed and an extracted pole section has been synthesized. Hence, the degree of all polynomials has reduced by one. The procedure will continue with as much sections as resonators in the topology.

Now, it is important now to consider how to end the synthesis in the last iteration, $k = N+1$. By looking at the nodal scheme in figure 3.8 and knowing that at each step an RN-NRN pair is extracted, it is obvious that at the last iteration a situation with a main line coupling (J_{N+1}) between two FIRs (B_N and B_L) will be faced, as in figure 3.12.

By chaining the $ABCD$ matrices of each element, it is found that $[ABCD]_{N+1}$ is

$$[ABCD]_{N+1} = \frac{1}{J_{N+1}} \begin{bmatrix} -B_N & j \\ j(J_{N+1}^2 + jB_nB_L) & -B_L \end{bmatrix} \tag{3.49}$$

And it is known that the remaining $ABCD$ matrix after the N-th step of the synthesis will be

$$[ABCD]_{N+1} = \frac{1}{jP_{N+1}(s)} \begin{bmatrix} A_{N+1}(s) & B_{N+1}(s) \\ C_{N+1}(s) & D_{N+1}(s) \end{bmatrix} \tag{3.50}$$

Note that now $P_{N+1}(s)$ has no remaining roots and thus, is a constant. Therefore, the evaluation of the three remaining elements shall be done at infinity. The first element to be extracted is J_{N+1}, and it will be computed as a cross-inverter at infinity.

$$J_{N+1} = \lim_{s\to\infty} -\frac{P_{N+1}(s)}{B_{N+1}(s)} = -\frac{P_{N+1}}{B_{N+1}} \tag{3.51}$$

After this, the updated $ABCD$ matrix is

$$\begin{aligned} [ABCD]'_{N+1} &= \frac{1}{jP'_{N+1}(s)} \begin{bmatrix} A'_{N+1}(s) & B'_{N+1}(s) \\ C'_{N+1}(s) & D'_{N+1}(s) \end{bmatrix} = \\ &= \frac{1}{j(P_{N+1}(s) + J_{N+1}B_{N+1}(s))} \begin{bmatrix} A_{N+1}(s) & B_{N+1}(s) \\ C_{N+1}(s) + 2J_{N+1}P_{N+1}(s) + J_{N+1}^2B_{N+1}(s) & D_{N+1}(s) \end{bmatrix} \end{aligned} \tag{3.52}$$

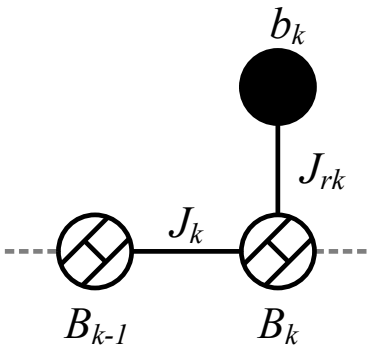

Figure 3.13: Nodal elements faced in the k-th iteration of the synthesis.

Now, FIR B_N must be extracted as a FIR at infinity with[9]

$$B_N = \lim_{s\to\infty} \frac{D'_{N+1}(s)}{B'_{N+1}(s)} = \frac{D'_{N+1}}{B'_{N+1}} \tag{3.53}$$

and the $ABCD$ matrix must be updated

$$\begin{aligned} [ABCD]''_{N+1} &= \frac{1}{jP''_{N+1}(s)} \begin{bmatrix} A''_{N+1}(s) & B''_{N+1}(s) \\ C''_{N+1}(s) & D''_{N+1}(s) \end{bmatrix} = \\ &= \frac{1}{jP'_{N+1}(s)} \begin{bmatrix} A'_{N+1}(s) & B'_{N+1}(s) \\ C'_{N+1}(s) - B_N A'_{N+1}(s) & D'_{N+1}(s) - B_N B'_{N+1}(s) \end{bmatrix} \end{aligned} \tag{3.54}$$

At this point only the load FIR B_L remains. To extract it, the network must be turned so to face it. Turning the network is possible by exchanging polynomials $A(s)$ and $D(s)$ in the matrix, as proposed by Tamiazzo and Macchiarella in [23]. After exchanging this polynomials, the computation of B_L involves applying another time (3.53) and (3.54). After updating this final extraction, the remaining $ABCD$ matrix should be empty and therefore the whole network should have been fully synthesized.

3.4.1 On the Need of Unitary Main Line Admittance Inverters

During the description of the synthesis procedure it has been stated that main line inverters are fixed to be unity and alternating in sign. To explain this, let us consider the elements present at a basic extraction step, as in figure 3.13, assuming that NRN element B_{k-1} has already been extracted.

The admittance of this section can be written as follows, being $Y_{rem}(s)$ the admittance of

[9] In (3.53) B'_{N+1} is polynomial $B'_{N+1}(s)$ but as it is of zero degree, has no frequency dependence. Must not be confused with any FIR element.

the subsequent sections of the network.

$$Y_{in}(s) = \frac{J_k^2}{jB_k + \dfrac{J_{rk}^2}{s + jb_k} + Y_{rem}(s)} \tag{3.55}$$

clearly this can be expressed as

$$\frac{J_k^2}{Y_{in}(s)} = jB_k + \frac{J_{rk}^2}{s + jb_k} + Y_{rem}(s) \tag{3.56}$$

what in turn can be expressed in a partial fraction expansion form, where the dangling resonator coupling J_{rk}^2 can be obtained as

$$J_{rk}^2 = J_k^2 \text{ residue} \left(\frac{1}{Y_{in}(s)} \right) \Bigg|_{s=j\Omega_k} \tag{3.57}$$

It is clear now that the value of couplings J_k and J_{rk} cannot be separately computed, but only their ratio. This allows a degree of freedom when setting one with respect to the other. In the scope of acoustic wave ladder filters, it has been introduced that main line admittance inverters are absorbed in the serialization of dangling resonators to series AW resonators. On the other hand, inverter J_{rk} is present in the definition of a dangling resonator resonance, and that is why the method involves fixing all J_k to unity and leaving J_{rk} to be computed. If needed, scaling of inverters can be applied after the network has been completely synthesized, without loss of generality.

However, one important issue must be contemplated. Note that in the extraction procedure, the last main line coupling has not been assumed as unity and has been extracted as a cross-coupling at infinity. This is mandatory for a proper conclusion of the synthesis, but imposes that this last admittance inverter J_{N+1} might not be unitary. For this inverter to be absorbed by its adjacent dangling resonator in the serialization, it must be ensured that $J_{N+1}^2 = 1$.

To tackle this, let us analyse the input admittance of the last step in figure 3.12.

$$Y_{in} = jB_N + \frac{J_{N+1}^2}{jB_L + G_L} \tag{3.58}$$

here, G_L is the output port conductance. As the network is normalized, $G_L = 1$. Let us enforce $J_{N+1} = 1$. Then, the expression can be separated in real and imaginary parts:

$$\mathrm{Re}(Y_{in}) = \frac{G_L}{B_L^2 + G_L^2} \tag{3.59a}$$

$$\mathrm{Im}(Y_{in}) = B_N - \frac{B_L}{B_L^2 + G_L^2} \tag{3.59b}$$

the new value of FIRs B_N and B_L must be found as

$$B_L = \pm \sqrt{\frac{G_L - G_L^2 \,\mathrm{Re}(Y_{in})}{\mathrm{Re}(Y_{in})}} \tag{3.60}$$

and

$$B_N = \mathrm{Im}(Y_{in}) + \frac{B_L}{B_L^2 + G_L^2} \tag{3.61}$$

If unitary load conductance is assumed (i.e. the network is matched) note that $\mathrm{Re}(Y_{in}) < 1$. If $\mathrm{Re}(Y_{in}) > 1$, B_L becomes purely imaginary what in turn, considering its FIR nature, would suppose a purely resistive element. These situations can be solved either by mismatching the network, fixing $G_L = 1/\mathrm{Re}(Y_{in})$ and leaving $B_L = 0$, or by adding an additional FIR element to somehow conform a matching network of two elements.

We have previously said that odd-order networks whose first and last TZ are equal can avoid both source and load FIRs by proper consideration of the phase. This means that $\mathrm{Re}(Y_{in}) = 1$ and thus $B_L = 0$. Furthermore, Ángel Triano, from the AMS group at UAB, in his forthcoming Ph.D. dissertation will present an asymmetric polynomial methodology that ensures $J_{N+1} = 1$ by means of the phase addition to $F(s)$.

3.5 Duplexer Considerations

The synthesis procedure presented is used to extract a network implementing a filter function and in section 3.3.2 the possibility to synthesize stand-alone filters avoiding source FIR by proper consideration of $\angle S_{11}(s)$ has been introduced. However, although stand-alone filters are of interest, it is common that they are implemented as part of duplexers connected to a single antenna used both for transmit (TX) and receive (RX) channels. The construction of a duplexer is not as simple as connecting together two filters designed individually to a common port, since each will experience the loading effects imposed by its adjacent filter.

Any signal input to the duplexer, will impinge at both the RX and TX filters of the duplexer. The RX-frequency signal that enters the TX filter branch will reflect at the input of this filter and will propagate back to the input of the RX filter where it will be able to go through[10]. However, at the input of this RX filter two signals will overlap: one that has propagated directly and the other that arrives after being reflected at the input of the TX. This overlap will cause an interference that might cause loss of signal integrity. If two filters are not designed carefully to construct a duplexer, this interference is the cause of a dramatic distortion of the filter responses. However, it is possible to impose some conditions to the network so that this interference is constructive and hence, does not distort the filter response.

Another time the procedure is focused on the input phase of the filter, i.e. $\angle S_{11}(s)$. In this case the objective is to force that each filter "*sees*" its counterpart as an open circuit at the

[10]This situation is completely equivalent to the one experienced by the signal coming from the TX to the antenna and its reflection at the input of the RX filter

centre of the so-called counter band (f_{CB}). This is that the RX filter acts as an open circuit at the centre of the TX band and viceversa. An open circuit condition is equivalent to an input phase of $\angle S_{11} = 0°$. In opposition to that shown in section 3.3.2, here we do not aim to avoid source FIR but to find the appropriate value of this FIR to ensure the open circuit condition.

Let us another time consider (3.39) but now at another evaluation point $s = j\Omega_{CB}$, namely the lowpass counter band frequency, resulting in

$$\theta_{CB} = -\arg\left(\left.\frac{F(s)/\varepsilon_r}{E(s)}\right|_{s=j\Omega_{CB}}\right) \tag{3.62}$$

Notice that $-\theta_{CB}$ is the inherent phase of the Generalized Chebyshev filter function at the centre frequency of the counter band. An important note is that in the mobile phone standards, the definition of bands is made from the handheld devide point of view. This is, RX bands are commonly the ones at higher frequencies and TX bands are below them.

Now polynomial $F(s)$ can be corrected using (3.38) and $\theta_{add} = \theta_{CB}$, and the synthesis procedure can continue as in the common case described in section 3.4. Thanks to this tailoring of the phase in the synthesis, a duplexer can be constructed just by the use of the inherent reactive input elements, thus avoiding the use of any additional phase shifters or transmission lines.

Notice that the imposition of the open circuit condition has been computed at Ω_{CB}. The phase is $0°$ at that exact frequency but this condition is not exactly met along the whole passband and therefore a slight alteration of the filter response will be experienced. Whereas, this is not a major concern since the distortion is small and the improvement in terms of device complexity and area are tangible.

3.6 Filter Example

To demonstrate the synthesis procedure explained above and its usability in acoustic wave filters, a duplexer design is described in this section. The proposed example is a Band 7 duplexer (IMT-E) and the objective mask specifications are summarized in table 3.3.

The frequency gap between bands is of 50 MHz, not a highly stringent specification compared with other duplexer pairs, but consider that due to temperature drifts and fabrication tolerances the gap might reduce. In this case a mask distortion figure of 800 ppm is considered as a general case. It is important to mention that the examples in this thesis are computed using a simple Q factor loss model [25] on the three elements of the BVD. This is by far the most general and also the most restrictive loss model. The use of the modified BVD

Table 3.3: Attenuation specifications of the Band 7 duplexer.

Specification	Frequency (MHz)	Magnitude (dB)
RX Insertion Loss	2620 - 2690	$>$ -2.6
TX Insertion Loss	2500 - 2570	$>$ -2.8
TX to RX isolation	2620 - 2690	$<$ -52
RX to TX isolation	2500 - 2570	$<$ -52
RX OoB rejection	2720 - 2900	$<$ -44
TX OoB rejection	2250 - 2450	$<$ -44

model is the common approach to model losses in electrical design but it is commonly part of the intellectual property of a company. A Q factor of 1500 for acoustic resonators and 50 for external coils has been considered.

In terms of the manufacturing material, the use of AlN will be considered yielding an objective k^2_{eff} in the range of 6.6% $\sim$ 6.9%. This range is considered as a general example. Although slight variations of k^2_{eff} might be acceptable, adaptation of an obtained coupling coefficient to the manufacturable material is also possible by the addition of external lumped elements in the laminate as explained in [19]. Additionally, in the scope of BAW resonators, a maximum number of 3 different resonances, and an extra tuning of one of them, will be considered. This is a common consideration in the industry, where it is possible to implement up to three different material thicknesses in the same wafer. The additional *resonance* is achieved via trimming of the thickness of the top metal electrode and thus is only a variation of one of the overall three.

Band 7 Receiver and Transmitter Filters

Let us initially present the design of the receiver filter of the duplexer. The transmission zero set is $\Omega_{TZ} = [\ 2.632, -2.223,\ 2.079, -2.074,\ 2.080, -2.228,\ 2.599]$ and return loss level of $RL = 18.9$ dB. Table 3.4 shows the synthesized elements of the Band 7 RX filter, figure 3.14a shows its response and figure 3.15a shows a closer view of the insertion losses to the filter. To fulfil the insertion loss specification an additional bandwidth of 0.822 MHz and 1.910 MHz in the lower and upper passband edges, respectively, has been added. For the transmitter filter, the transmission zero set is $\Omega_{TZ} = [2.029, -2.195,\ 1.987, -2.011,\ 1.987, -2.195,\ 2.029]$ and return loss level of $RL = 20$ dB. See the synthesized BVD elements of the Band 7 TX filter in table 3.5. Its response is depicted in figure 3.14b and figure 3.15b shows the in-band losses. Another time, a bandwidth enlargement of 0.422 MHz and 1.510 MHz has been applied respectively to the lower and upper passband edges.

Table 3.4: BVD elements of the Band 7 RX filter.

Resonator	1	2	3	4	5	6	7
L_a (nH)	90.0236	12.6081	111.2312	12.0135	111.2591	12.5606	90.4507
C_a (pF)	0.0393	0.3033	0.0323	0.3170	0.0323	0.3045	0.0391
C_0 (pF)	0.6703	5.1232	0.5358	5.3089	0.5355	5.1292	0.6781
L_{in} (nH)	3.075						
L_{out} (nH)	3.712						
k^2_{eff}	6.73	6.79	6.91	6.85	6.91	6.81	6.63
f_s (GHz)	2.676	2.573	2.655	2.578	2.655	2.573	2.676

Table 3.5: BVD elements of the Band 7 TX filter.

Resonator	1	2	3	4	5	6	7
L_a (nH)	78.2403	21.6467	171.4736	20.4977	171.4712	21.6507	78.2495
C_a (pF)	0.0503	0.1940	0.0230	0.2038	0.0230	0.1940	0.0503
C_0 (pF)	0.8375	3.2530	0.3853	3.4177	0.3853	3.2529	0.8373
L_{in} (nH)	15.491						
L_{out} (nH)	15.483						
k^2_{eff}	6.89	6.84	6.84	6.84	6.84	6.84	6.89
f_s (GHz)	2.536	2.456	2.535	2.4322	2.535	2.456	2.536

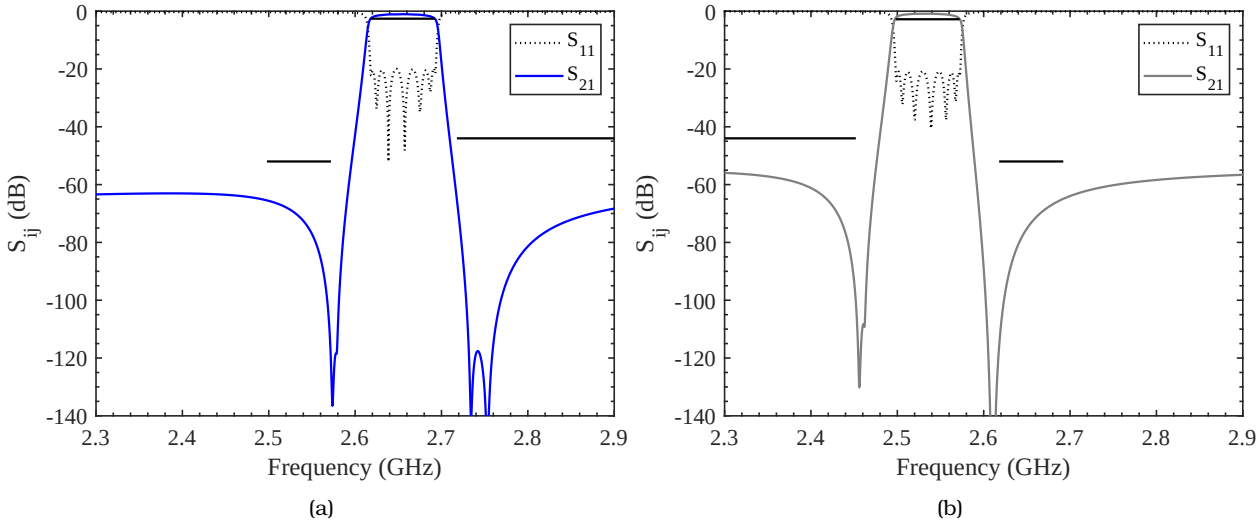

Figure 3.14: Magnitude response simulation of the Band 7 filters. (a) Receiver channel, (b) Transmitter channel.

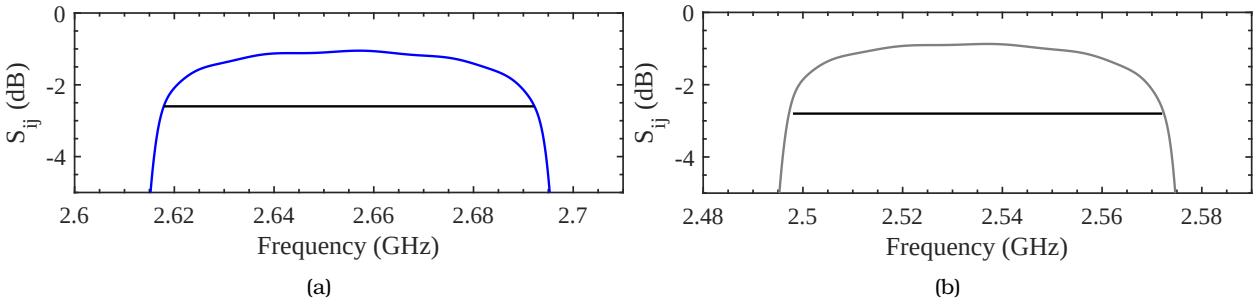

Figure 3.15: Insertion loss close-up of the Band 7 filters. (a) Receiver channel, (b) Transmitter channel.

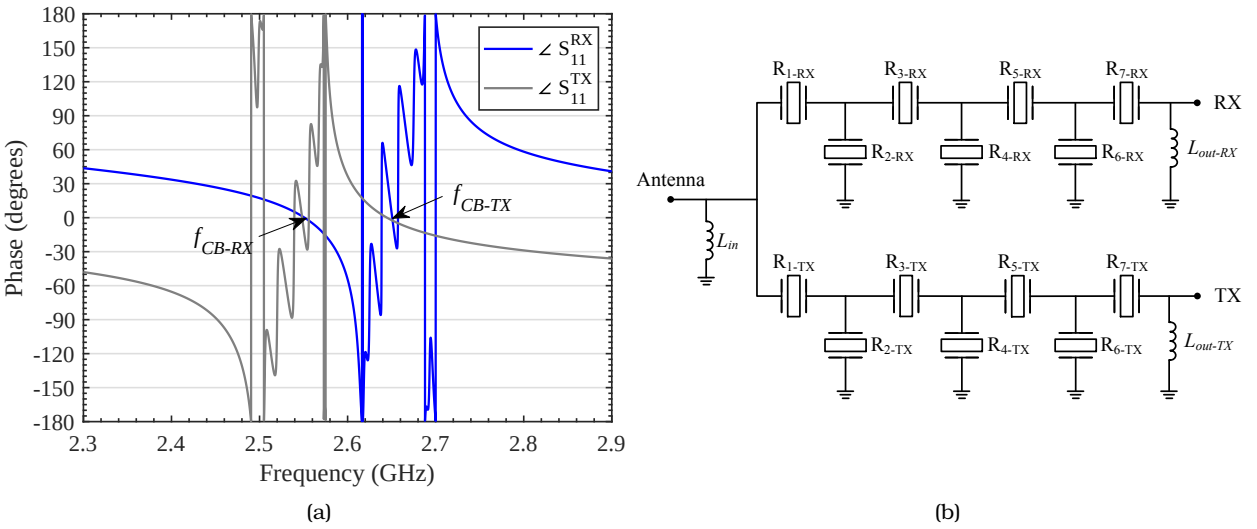

Figure 3.16: (a) Input phase of the two filters of the Band 7 duplexer, (b) Schematic of the Band 7 duplexer.

Band 7 Duplexer

Since we are designing a duplexer, the considerations explained in section 3.5 need to be applied. Prior to the synthesis, the phase of the filtering function has been tailored to depict an open circuit at the centre frequency of the counter band of each filter. Figure 3.16a depicts the phases of the two filters designed and proofs that after transformation they implement a phase of $0°$ at the centre of their respective counter bands.

Therefore, the two filters can now be connected to conform a duplexer. The final schematic of the duplexer is shown in figure 3.16b. Note that since both filters feature a shunt input inductor, the two can be merged in parallel to create a common inductor at the antenna port. The final magnitude response of the two filters jointly connected and their insertion loss close-up are shown in figures 3.17 and 3.18 respectively.

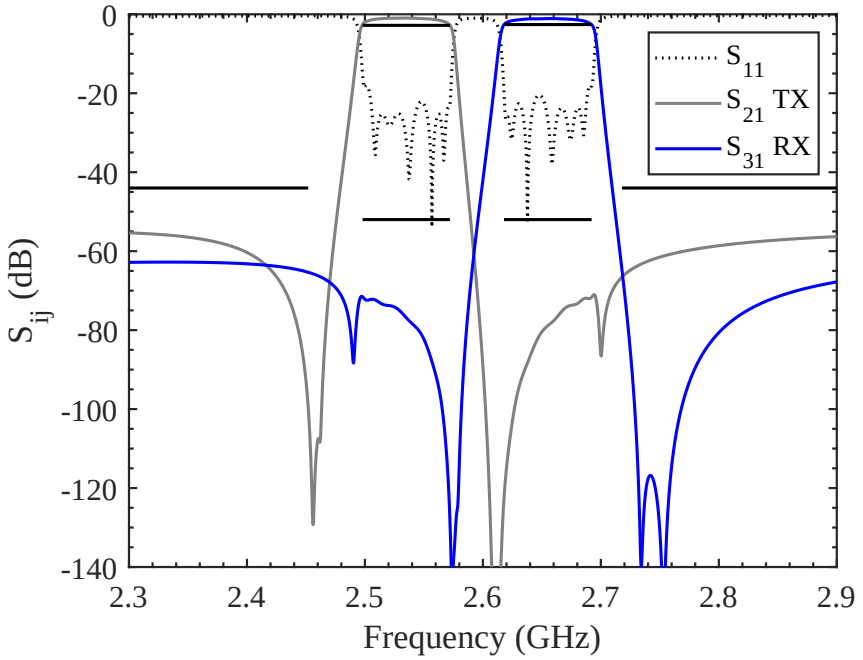

Figure 3.17: Magnitude response simulation of the Band 7 duplexer.

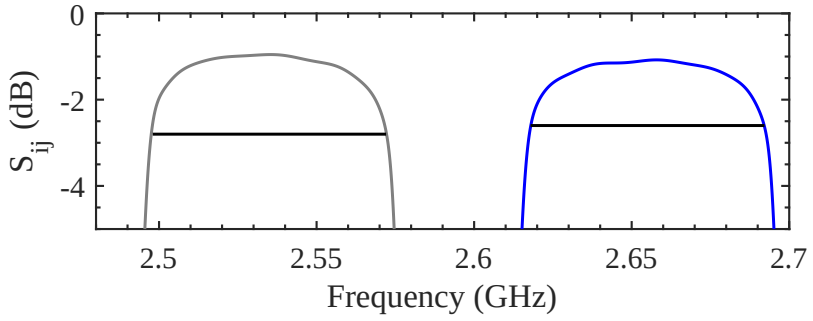

Figure 3.18: Insertion loss detail simulation of the Band 7 duplexer.

Chapter 4

Considerations for Filters Starting in Shunt Resonator

The previous chapter provided a full description of the synthesis procedure of acoustic wave ladder filters. The most typical schematic of these filters is the one shown in the initial figure 2.6, an odd-order network where the first and last resonators are in series configuration. Since each resonator is responsible for a transmission zero, these filters depict one more zero in the upper stop-band than in the lower and therefore its upper out-of-band rejection is enhanced. Nevertheless, better OoB rejection at the lower stop-band might be desired for multiple reasons, for example to increase isolation with respect to the transmitter side of a duplexer (recall that the TX side is commonly at a frequency below the RX) or to increase rejection of a closely located band. To achieve this, it is interesting to consider a network whose first resonator is in shunt configuration, hence prescribing more zeros at the lower stop-band.

This approach has been exploited in the industry, but if inspected, the use of shunt-starting networks in the market leads to an interesting observation: the typical configuration of these filters includes two reactive elements at the input of the filter, one shunt and one series. The need of the input and output reactive elements has been introduced in section 3.3.2, but in that case, a single element was needed. A reference case of this situation is observed in the paper by Link and Warder [4]. In this paper the authors show a general schematic of a Band 25 duplexer manufactured by TriQuint (nowadays Qorvo), reproduced in figure 4.1 for explanation purposes. Observe that both filters start in shunt resonator and the TX clearly features two reactive elements at the input. The RX appears to feature a single one but the authors comment that its input shunt capacitor is implemented by the first resonator of the TX filter.

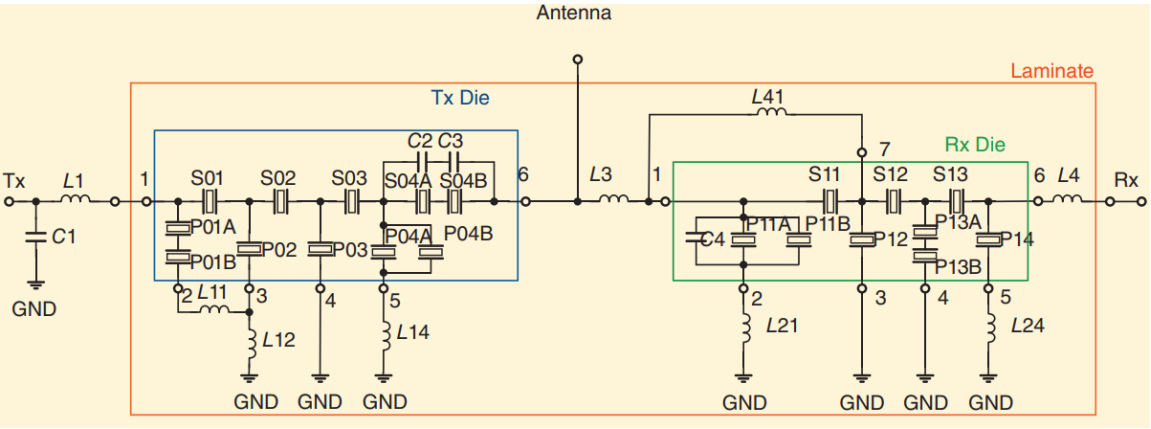

Figure 4.1: Band 25 duplexer schematic extracted from [4] (Figure (j) on page 66, IEEE Microwave Magazine ©, August 2015). Both filters start in shunt resonator and feature multiple reactive elements at the input/output.

It is now clear that shunt-starting acoustic wave filters need of careful consideration when designing. This chapter aims to provide a synthesis vision of the situation and considerations to help designers achieve feasible solutions.

4.1 Nodal Representation of a Shunt-Starting Acoustic Wave Ladder Network

To correctly synthesize a ladder network starting in shunt resonator, the first step is to take a look another time at the nodal representation of the network shown in figure 3.8. In the case of series-starting networks, following the general procedure described in section 3.4, since the first resonator is series, admittance inverters J_1 and J_6 are absorbed by their adjacent resonators to attain serialization purposes following (3.37). Therefore, extracted FIRs B_S and B_L are transformed to shunt reactive elements, either inductive or capacitive depending on their sign. Let us assume now the synthesis of a network like that but where first and last resonators are shunt. It is clear, that inverter J_1 will not be absorbed by the first resonator and thus, the input remaining elements will be a shunt FIR B_S and the inverter J_1. The situation is the same in the load node.

In acoustic wave technology the physical implementation of an admittance inverter, either by a π or T topology of lumped elements, is not feasible and therefore inverter J_1 must be dealt with prior to implementation. Observe that for the topology to be a complete ladder, the input and output reactive elements should be series and this could be achieved if an extra admittance inverter was present between network input and input FIR. The need of this extra

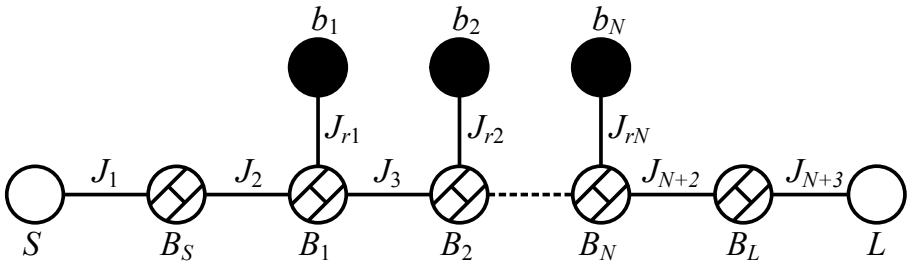

Figure 4.2: Lowpass nodal representation of an odd-order shunt-starting acoustic wave ladder network.

inverter is mandated by the fact that all main line admittance inverters must be absorbed to serialize elements and cannot be implemented. Therefore, the proposed nodal representation of an odd-order shunt-starting network results in the one shown in figure 4.2.

All elements are the same as in chapter 3 but now source and load NRNs are placed between admittance inverters. White nodes S and L are the input and output terminals of unitary conductance value $G = 1$. In the case of series-starting networks, FIR $B_{S/L}$ and terminals were superposed.

4.2 Extraction of the Shunt-Starting Network

Given the new nodal representation depicted in the previous section, the synthesis procedure described in section 3.4 has to be slightly modified at iterations $k = 1$ and $k = N + 1$. At the first iteration, the modification is minimum as only the extraction of an additional admittance inverter is needed. The whole first iteration consists in extracting a unitary inverter J_1 using (3.45), then B_S with (3.43) and (3.44), now another time a unitary inverter J_2 of opposite sign than J_1 (main line inverters have been defined as alternating in sign) using another time (3.45) and then J_{rk}^2 with (3.47) and (3.48).

4.2.1 Last Iteration

In terms of the last iteration, the modification is not too complex, but implies a couple of extra steps. It has been defined in the previous chapter that in the last iteration all elements were extracted at infinity as the degree of $ABCD$ polynomials is zero and there are not roots of $P(s)$ left. In this case the situation is the same in terms of degree, but recall that the extraction of the main line inverter between B_N and B_S is evaluated as a cross-inverter at infinite frequency. As depicted in figure 3.10, if a cross-inverter is evaluated when facing the last iteration it would connect FIR B_N with output terminal L, imposing an actual cross-

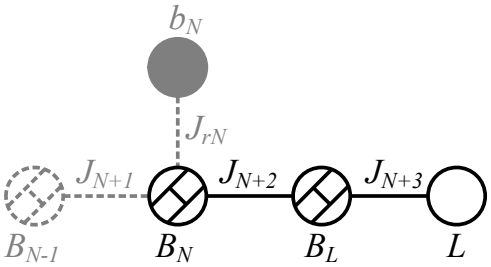

Figure 4.3: Iteration $k = N + 1$ of the synthesis procedure on an odd-order shunt-starting network.

coupling parallel to the mainline. This cross-coupling cannot be contemplated for the network to be a pure ladder. To evaluate this coupling between B_N and B_L, admittance inverter J_{N+3} must be extracted a priori. The situation that is faced at this iteration is shown in figure 4.3.

As proposed by Tamiazzo [23], a turn in the reference point of the network is equivalent to exchanging polynomials $A(s)$ and $D(s)$. Thus, when the last iteration is faced, the first step is to turn the network, $A(s) \leftrightarrow D(s)$, then extract J_{N+3} taking its sign in consideration, as in (3.45) and then turn the network another time to go back to the position of B_N. At this point, the cross-inverter at infinity J_{N+2} can be extracted using (3.51) and (3.52), then B_N is obtained with (3.53) and (3.54), and the network is turned another time to face B_L and repeat the operation.

With this, the synthesis steps have been refined to accurately contemplate a network starting and/or ending in shunt resonator. It is important to note that single input and output elements are considered up to now.

4.3 Feasibility Regions of Acoustic Wave Ladder Networks

Let us consider a 7-th order fully canonical network with prescribed transmission zeros $\Omega_{TZ} = [-1.7,\ 1.97, -2.5,\ 3, -3.3,\ 4, -1.2]$, return loss level of $RL = 18$ dB and a phase addition $\theta_{add} = 0°$, that is, leaving the inherent phase of the Chebyshev function. The lowpass elements output by the synthesis are depicted in table 4.1.[1]

It is important to notice the sign of elements B_1 and B_7. From (3.31) and the transformation from dangling resonator to lowpass BVD in (3.36) and (3.37), the expressions relating C_0 and

[1]The results in the table correspond to the output of the synthesis before proceeding with the redistribution of the last main line admittance inverter, namely J_{10}, to be unitary as in (3.59). In fact, redistributing J_{10} might turn B_7 positive hence partly masking the phenomena we aim to describe.

Resonator	B_k	b_k	J_{rk}
1	-0.1261	1.7	0.8244
2	-7.2909	-1.97	3.5159
3	1.4959	2.5	1.9526
4	-14.1572	-3	6.4863
5	2.0471	3.3	2.6182
6	-14.1179	-4	7.3840
7	-0.0685	1.2	0.4170
B_S	-1.4332		
B_L	-0.5108		
J_{10}	-0.6963		

Table 4.1: Lowpass synthesized elements of the 7-th order network of $RL = 18$ dB and $\Omega_{TZ} = [-1.7,\ 1.97, -2.5,\ 3, -3.3,\ 4, -1.2]$.

B_k can be rewritten as follows, considering that $J_k^2 = 1$.

$$C_{0-SE} = -\frac{1}{\omega_0 B_k Z_0} \tag{4.1a}$$

$$C_{0-SH} = \frac{B_k}{\omega_0 Z_0} \tag{4.1b}$$

This expressions define that the sign of the FIR elements B_k is of paramount importance to allow the transformation to the BVD model of the acoustic resonator. For series resonators, $B_k < 0$ and conversely, for shunt resonators $B_k > 0$. Therefore, in a ladder topology, the sign of B_k elements alternates. Then, it is clear that the synthesized example in table 4.1 cannot be transformed to a BVD model since the static branches of the first and last resonators are not capacitive but inductive: the synthesized filter is not feasible in the acoustic domain.

In order to understand why does the network require a negative sign for these FIR elements, we will make use of the input phase of the filter with the additional phase term θ_{add}. As we have seen that the role of main line FIRs is fixing the correct phase condition at each extracted pole section, modification of the input phase of the filter via polynomial $F(s)$, as done for the synthesis of stand-alone filters in (3.39), will impact the values of the static capacitance of all resonators in the ladder. Therefore it is interesting to assess how does the nature of B_k elements change with respect to the input phase. For a complete comprehension of the situation, let us also keep in mind the orthogonality condition in (3.13) that mandates how an input phase shift is asymmetrically absorbed by parameters $S_{11}(s)$ and $S_{22}(s)$.

Let us consider another time the 7-th order network from the beginning of the section and

for exemplification purposes imagine an arbitrary counter band at $\Omega_{CB} = -2.34$ rad/s. This would be the case of trying to implement a network as an RX filter, thus having its counter band in the lower stop-band. Now, the experiment consists in performing the synthesis of the network for a sweep of the entire range of additional phase values, $\theta_{add} \in [-180, 180]$ degrees. After computing the synthesis and before redistributing the last main line admittance inverter, the sign of all B_k elements is checked to yield a positive C_0. This allows to construct a binary feasibility map like the one depicted in figure 4.4.

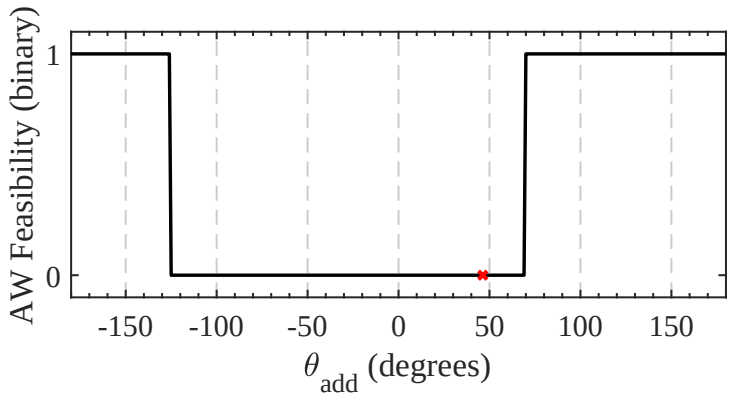

Figure 4.4: Feasibility map of the 7-th order shunt-starting network described above. Binary (1) indicates all B_k have their expected sign, (0) is first and/or last resonator have $B_k < 0$. Red cross is placed at the phase requirement for duplexer synthesis at $\Omega_{CB} = -2.34$ rad/s.

The feasibility map indicates that the example network is only feasible for large values of θ_{add} and not for the intrinsic phase of the Generalized Chebyshev filter function. Moreover, in the current example, the phase requirement to fix the duplexer condition denoted in (3.62) falls inside the non-feasible region (red cross in figure 4.4).

For a more complete view of the situation, let us repeat the experiment but now also sweeping the position of the first transmission zero to positions further from the passband (i.e. more negative values of Ω_1). Consider the same network than before and test the cases were $\Omega_1 = [-1.7, -3.4, -4.8, -6.7, -9.2]$. Another time a feasibility map is computed and shown in figure 4.5. This experiment shows that the upper edge of the feasibility region changes with the position of the first transmission zero, coming closer to $\theta_{add} = 0°$ as the zero moves further from the passband.

We conclude that the further the first TZ, the smaller the non-feasible region, even allowing the synthesis of a duplexer at some point. By careful inspection and making use of (3.13) and (3.38), it can be found that the lower and upper edges of feasible regions are the phase correction values needed for source and load element avoidance respectively. In other words,

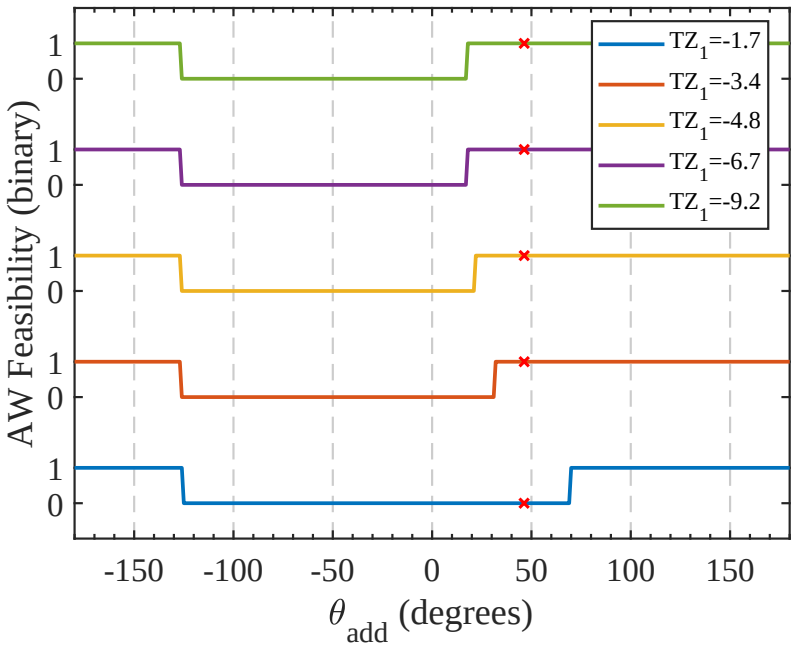

Figure 4.5: Feasibility map of the 7-th order shunt-starting network sweeping Ω_1. Red cross is placed at the phase requirement for duplexer synthesis at $\Omega_{CB} = -2.34$ rad/s.

this can be expressed as[2]

$$\theta_{up-SH} = -\angle S_{11}(j\Omega_1) \qquad \text{and} \qquad \theta_{low-SH} = \angle S_{22}(j\Omega_N) \tag{4.2}$$

As has been shown in section 3.3.2, by adding a shift of θ_{up} to $F(s)$, then $\angle S_{11}(j\Omega_1) = 0°$ and therefore no source FIR element B_S is needed. Expression (4.2) allows to compute in advance the feasibility region of a given odd-order network starting in shunt resonator. Additionally, plots in figures 4.4 and 4.5 show us that a shunt-starting network is only feasible when $\angle S_{11}(j\Omega_1) > 0$. Therefore, from the perspective of a duplexer whose counter band is placed below the passband, it is seen that only networks whose first TZ is further than the counter band will be feasible with a single input element since two conditions must be met: $\angle S_{11}(j\Omega_1) > 0$ and $\angle S_{11}(j\Omega_{CB}) = 0$. Thus, the following condition can be derived for shunt-starting networks at the receiver side of a duplexer

$$\Omega_1 < \Omega_{CB} \tag{4.3}$$

For the sake of completeness, it is also interesting to inspect how do odd-order networks starting in series behave. To do so, let us consider the same set of transmission zeros but inverting the sign of all of them and the same return losses of 18 dB. Proceeding with the synthesis method explained for series-starting networks, that is without considering any additional admittance inverter, the network yields a feasible result without adding any phase

[2] SH subscript indicates this is the shunt-starting case.

to polynomial $F(s)$. The previous experiment is repeated now sweeping all θ_{add} and for $\Omega_1 = [\ 1.7,\ 3.4,\ 4.8,\ 6.7,\ 9.2]$. The resulting feasibility map is depicted in figure 4.6.

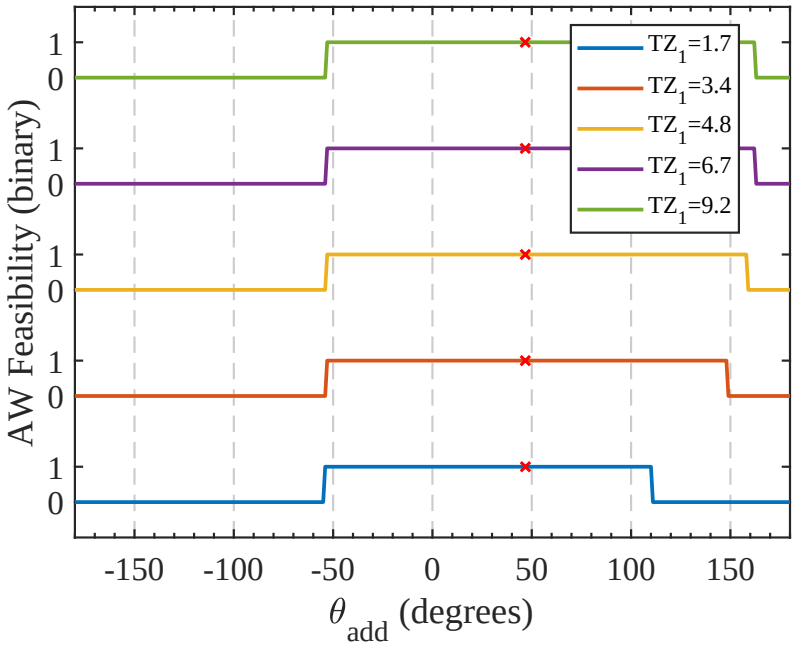

Figure 4.6: Feasibility map of the 7-th order series-starting network sweeping Ω_1. Red cross is placed at the phase requirement for duplexer synthesis at $\Omega_{CB} = -2.34$ rad/s.

Surprisingly, series-starting networks show feasibility regions similar to those of shunt-starting networks, but with a complementary behaviour. Now the feasible region is centred around $\theta_{add} = 0°$, what indicates that the ladder structure with single elements at input and output is naturally capable of accommodating Generalized Chebyshev filter functions without the need of any phase correction or extra element extraction if the first and last resonators are placed in series. Moreover, the feasible region for series-starting networks includes the duplexer phase condition, what explains why starting in series is the common option for implementation since the feasible solutions arise in the proper phase range for most duplexer-pair filters.

In this case, the upper and lower edges of the regions are still related to the position of the TZs as [3]

$$\theta_{up-SE} = 180 - \angle S_{11}(j\Omega_1) \qquad \text{and} \qquad \theta_{low-SE} = -180 + \angle S_{22}(j\Omega_N) \tag{4.4}$$

Having identified the appearance of feasibility regions for the synthesis of both series- and shunt-starting networks, now the reason for their existence must be addressed. Two main conclusions can be drawn from the situations exposed:

[3] SE subscript indicates this is the series-starting case.

Firstly, the fact that non-feasible regions are centred around $\theta_{add} = 0°$ for shunt-starting networks is closely linked to the behaviour shown by their series-starting counterparts. Let us explain this: We have concluded that a nodal scheme like the one shown in figure 3.8, applicable to an acoustic network starting in series resonator, is intrinsically capable of implementing a Chebyshev response. However, we have also found that for the same nodal representation there are phase values for which the output of the synthesis is not feasible in terms of acoustic wave technology. These limits are stated in (4.4). Now, observe that the only difference between the nodal scheme proposed for shunt-starting networks in figure 4.2 and that for those starting in series in figure 3.8 is that two additional admittance inverters, J_1 and J_{N+3}, have been placed, imposed by the serialization of source and load FIRs. By comparing (4.4) and (4.2), it can be seen that there is a $180°$ difference between them. Clearly, the addition of the two admittance inverters has moved the non-feasible regions of the series-starting network down to the center of the plot, that is, around the intrinsic phase of the Chebyshev function. Another time using (3.13), note that adding these two inverters is a change of $+180°$ in S_{11} and $-180°$ in S_{22}.

Secondly, the reason why FIR elements B_1 and B_N are synthesized with the opposite value to that desired can be inspected from both types of network, but for the sake of simplicity it will be addressed from a series-starting case. We have just shown that one case is a shift of the other. Consider the network that has been used for the experiment in figure 4.6, that is $RL = 18$ dB and $\Omega_{TZ} = [\ 1.7, -1.97,\ 2.5, -3,\ 3.3, -4,\ 1.2]$, and let us use $\theta_{add} = 180°$. Since this phase is outside the boundaries in (4.4), the result will for sure be non feasible. Figure 4.7a shows the phase of the Generalized Chebyshev function with that phase addition. The synthesis for this network results in $B_1 = 0.1261$ and $B_7 = 0.0685$. These two values should be negative.

Note in figure 4.7a that the phase evaluated at the first TZ, $\Omega_1 = 1.7$ is negative. Therefore, the value of source FIR B_S is positive, $B_S = 1.4332$. See now in 4.7b, that at the moment of extracting B_1, the phase at $\Omega_2 = -1.97$ is also negative, therefore yielding a positive FIR, $B_1 = 0.1261$. This is the change in sign of the first FIR. Note now that after the second extracted pole section (figure 4.7c) the phase is now even more negative. Thus, when extracting the third FIR at $\Omega_3 = 2.5$, we obtain $B_3 = 0.7209$, in order with what is expected for a series resonator. For all the remaining sections, each FIR complies with the desired sign as $\angle S_{11}(j\Omega_k)$ will alternate between positive and negative values for each synthesis step. If the function had not been altered with a $180°$ phase, after the extraction of the first extracted pole section, the phase would be positive - similar to that in figure 4.7c but in the upper half of the plot - and would yield a negative FIR value for B_1. At each iteration the phase would alternate between the

upper and the lower halves of the phase plot, yielding the expected signs for NRNs. Now, observe the situation in 4.7d. This is the remaining phase at the moment of starting the last iteration. We have seen in section 3.4 that this last iteration involves evaluation of the FIRs at infinity because the $ABCD$ polynomials are of zero degree. After extracting the cross-inverter at infinity, the evaluation of the seventh FIR yields a positive value $B_7 = 0.0685$ and then, after turning the network, $B_L = 0.5108$. Note that at the last iteration the phases of S_{11} and S_{22} are of opposite sign. The fact that $\angle S_{22}$ is negative imposes that element B_7 is positive and hence, non-feasible. Conversely, for the same series-starting network if no phase had been added to $F(s)$, at the last iteration both phases would be positive and yield that both FIRs, B_7 and B_L are negative.

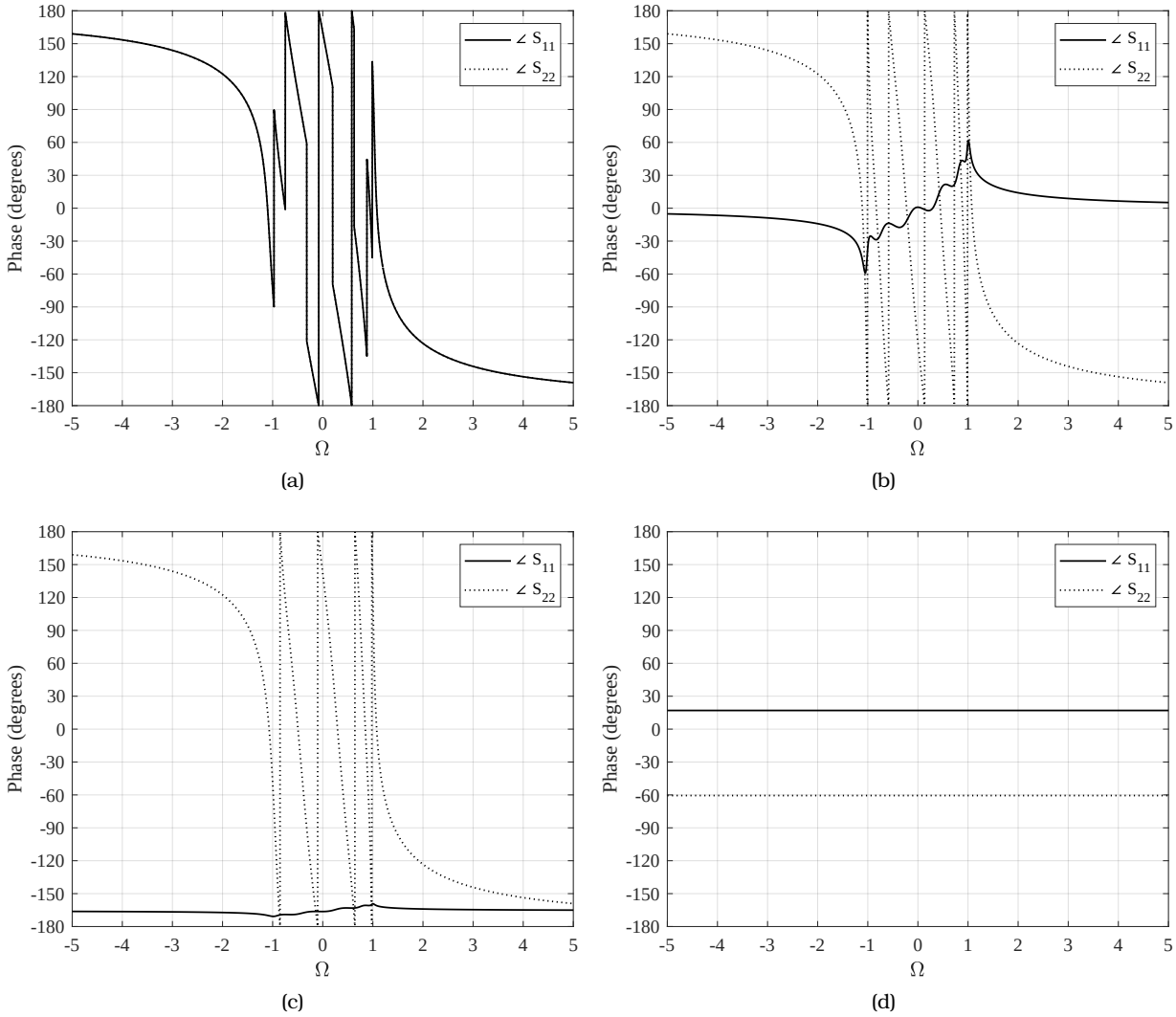

Figure 4.7: Phase of the series-starting example network along the synthesis. (a) Intrinsic phase of the Gen. Chebyshev function with $\theta_{add} = 180°$, (b) After extraction of the first resonator, (c) after the extraction of the second resonator, (d) facing the last iteration.

4.4 Synthesis Considerations

After having exposed all the reasons why shunt-starting ladder networks must be carefully handled, this section aims to provide design recommendations and examples for the design of these filters.

4.4.1 Stand-Alone filters

Firstly, let us address the design of a filter that is not part of any duplexer or multiplexer device. It has been shown in section 3.3.2 that a proper phase correction of $F(s)$ allows to avoid the input reactive element in series-starting networks. For those starting in shunt the expression also applies. Notice that the upper edge of the shunt-starting feasible region in (4.2) is exactly the phase at which the input element is avoided. Therefore, these networks will always be transformable to a ladder of BVD models. In terms of lowpass element extraction, when this phase condition is imposed, $B_S = 0$ for series-starting and $B_S = \infty$ for shunt-starting networks. Obviously, a zero-valued shunt admittance and an infinite-valued series admittance respectively.

Moreover, avoiding the input element is not the only option for stand-alone filters. By keeping both input and output elements the additional degree of freedom of the input phase is enabled. To search for a filter solution fulfilling technological requirements does not only involve tuning the zeros and return losses of the function but also brings the phase addition term θ_{add} into play. It has already been commented that altering the phase of $F(s)$ imposes an alteration on the values of all static capacitances of the ladder, and so, on the effective coupling coefficient required.

4.4.2 Duplexers filters and the Double-Element Solution

For the synthesis of duplexers, the main conditions have already been explained in section 3.5. The role of the input phase in the prescription of the open circuit condition at the centre of the counter band is the basic step when synthesizing a duplexer. However, we have already seen in figure 4.5 that depending on the position of the first transmission zero, the duplexer phase condition might fall outside the feasible region and therefore impede the synthesis of the filter. Based on this, the condition in (4.3) has been derived. Fulfilling this condition will ensure that the required phase for duplexer synthesis will fall into the feasible zone but does not ensure that the obtained solution will fulfil technological constraints such as a constant k^2_{eff} along the filter. Tuning of zeros (considering the imposed condition) and return loss can

be applied to search for a final solution, but note that in this case the degree of freedom of the phase is not enabled since it is fixed at θ_{CB} from (3.62).

As an example, figure 4.8, shows the band 7 duplexer in chapter 3 now featuring a 7-th order shunt-starting filter at the receiver side. Note the enhanced rejection at the lower band. This figure is shown as a proof example of the modified synthesis procedure for shunt-starting networks. Accommodating technology limitations in this filter example would require further tuning of parameters by means of this synthesis procedure.

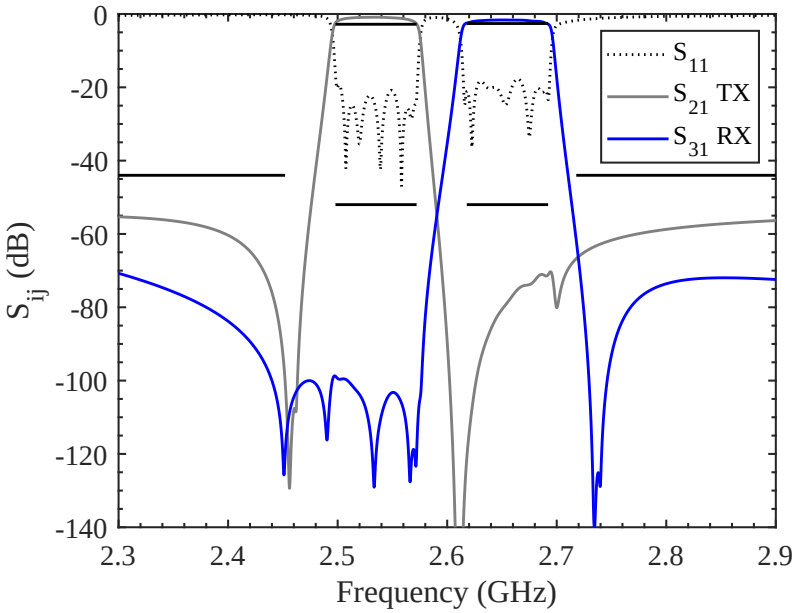

Figure 4.8: Example of a receiver filter starting in shunt for the Band 7 duplexer in chapter 3. Transmitter side is the same as before.

From the fact that (4.3) must be imposed, the search of a shunt-starting AW filter fulfilling both duplexer condition and technological requirements with a single input element might become a challenging synthesis and design task. A first transmission zero placed at such a distant position is clearly linked to resonators with a high value of k^2_{eff} and without the phase degree of freedom, intense search is required to find a solution. Nevertheless, in figure 4.1 we have seen that solutions by the industry featured more than a single input element. Considering all the limitations to take into account for shunt-starting networks it is clear that overcoming all of them by hard optimization effort over a predefined topology with single input elements might not be possible. Consider for example that (4.3) is not fulfilled. Optimization will not find a feasible solution. However, by adding an additional input element, solutions might be found. In the coming lines we will provide a synthesis view of the double-element solution.

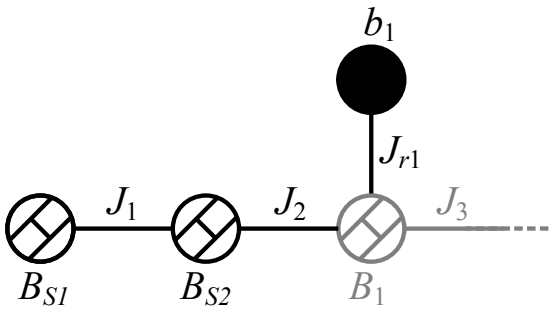

Figure 4.9: Nodal representation of the first iteration of the synthesis of a double-element solution.

Start by considering the nodal representation in figure 4.9. This corresponds to the first iteration of the synthesis if two input elements are allowed. Let us now identify which is the role of them. We have seen in (3.43) how a B_k element is obtained at each iteration as a preparation for the upcoming dangling resonator section extraction. If the value of B_{S1} is now faced the same way, the synthesis will not converge since B_{S1} will take the value as if we were performing a common series-starting synthesis, and B_{S2} would be 0. However, what if the value of this extra input element is tailored in advance, extracted from the $ABCD$ polynomials and then the synthesis resumes? Firstly, we shall find which is the phase implemented by an arbitrary input FIR element.

We may inspect the phase as $\angle S_{11}(j\Omega_1)$ and it is known that

$$Y_{in}(s) = \frac{1 - S_{11}(s)}{1 + S_{11}(s)} \tag{4.5}$$

For the general case of the shunt-starting network (this computation yields the same result if applied to a series-starting network) we can find the input admittance expression as

$$Y_{in}(s) = \cfrac{J_1^2}{jB_S + \cfrac{J_2^2}{jB_1 + \cfrac{J_{r1}^2}{s + jb_1} + Y_{rem}(s)}} \tag{4.6}$$

By applying (4.5) and (4.6), and evaluating at $s = j\Omega_1 = -jb_1$ it is found that the phase implemented by the source FIR is

$$\angle S_{11}(j\Omega_1) = \arctan\left(\frac{2B_S}{B_S^2 - 1}\right) \tag{4.7}$$

It has been shown in figure 4.7 how the phase depicted at any step of the synthesis imposed the sign of B_k elements. For a non-feasible network, the input phase after the first iteration is such that forces B_1 to change in sign. Now, the procedure is to manually define a phase to be implemented using B_{S1}, and compute the element using (4.7). This expression is a second order equation with two solutions of different sign. The positive one will transform to a shunt

capacitor C_{in} and the negative will transform to a shunt inductor, L_{in}. By extracting B_{S1} from the $ABCD$ polynomials with (3.43), the synthesis procedure can resume with the extraction of J_1, then B_{S2}, and so on. If the phase implemented by B_{S1} is properly considered, the network becomes feasible for an arbitrary set of zeros not fulfilling (4.3). This might be understood as if element B_{S1} brings the remaining network into the feasible region.

For exemplification purposes, let us work another time on the network at the start of this chapter. The transmission zero set is $\Omega_{TZ} = [-1.7,\ 1.97, -2.5,\ 3, -3.3,\ 4, -1.2]$ and we will use a return loss level of $RL = 20$. If it is to be designed as the RX filter of the Band 7 duplexer, its counter band is located at $\Omega_{CB} = -3.105$. At this frequency, the synthesized Generalized Chebyshev function has a phase of -34.45 degrees. That means necessary phase addition $\theta_{CB} = 34.45°$ and clearly, this falls out the feasible region in figure 4.4. To apply the double-element solution let us fix a phase of 60 degrees to be implemented by B_{S1}. This value is arbitrary and is only used as a proof of concept. Finding a solution fulfilling technological constraints would imply fine tuning of this predefined phase. Note that thanks to this additional element, the degree of freedom of the phase is brought back to the synthesis procedure of duplexers. Solving (4.7) for 1.0472 radians (i.e. 60 degrees) yields two solutions: -0.5774 and 1.7321. In this case we have chosen the first, to implement the FIR as a shunt inductance. Then, B_{S1} is extracted and the synthesis can proceed. The extracted value of B_{S2} is -1.116, yielding a series capacitor, and the first and last B_k are now $B_1 = 0.1001$ and $B_7 = 0.6359$. Both positive, as desired to allow transformation to the BVD model. After bandpass transformation, the response of the whole duplexer can be simulated and is depicted in 4.11. Its final schematic is depicted in figure 4.10. As before, the two shunt inductor elements can be merged into a common port node.

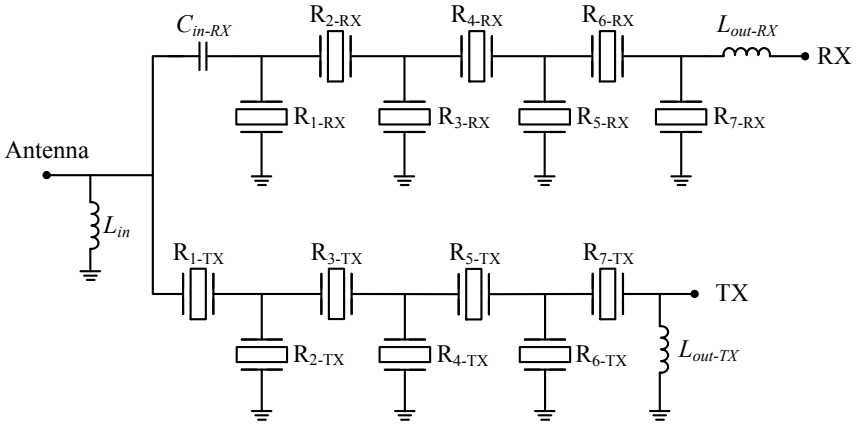

Figure 4.10: Schematic of the Band 7 duplexer.

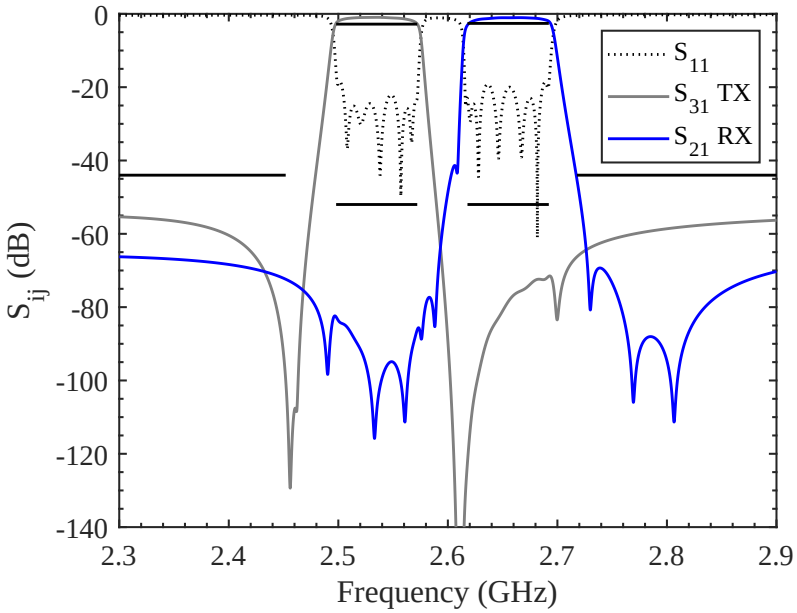

Figure 4.11: Simulation response of the Band 7 duplexer with double-element RX filter.

Chapter 5

Conclusions

In this thesis the fundamental paper of acoustic wave technology in microwave filters for mobile communications has been presented as the encouraging factor to study and develop filter synthesis methodologies. The unstoppable pace of the mobile communications industry in combination with the vast activity in the microwave filters field of research, deem the link between the two worlds a topic of great interest.

In the prior work by the Antenna and Microwave group at UAB, the synthesis of acoustic wave filters has commonly been presented on the most general acoustic wave ladder topology, one that starts in series resonator. In this work, apart from presenting the relation between acoustic wave filters and their lowpass representation from a synthesis point of view, the objective is to face the case of networks whose first resonator is in shunt configuration. Since the final implementation technology is always kept in mind, the handling of such networks has prompted feasibility issues. These issues have been exposed and discussed and different solutions have been proposed.

The general design of stand-alone filters without input element thanks to the input phase of the network, stand-alone filters with input element bringing the input phase into play to find technologically feasible solutions, the role of the input phase on the avoidance of loading effects for the construction of duplexers, rules on the prescription of transmission zeros for shunt-starting duplexers featuring a single input element and the synthesis view to the double element solution to ease the search of manufacturable solutions. All these cases have been contemplated in this work after having introduced the foundations of lowpass network representation.

On top of that, all the steps presented in this thesis have been implemented in a proprietary software tool aimed for acoustic filter designers. A tool that unifies under a controlled environ-

ment many steps that are commonly addressed by optimization in the industry. Therefore, a valuable aspect of this work is its intention to provide the industry with knowledge that helps improving its competitiveness. For example, the definition of the feasibility regions of acoustic wave filters, both series- and shunt-starting is a way to assess in advance which solutions can not be obtained by optimization.

In terms of future lines, many topics covered in this thesis are of interest for further research. Among others, initially it might be interesting the manufacture of a prototype with an equivalent technology to demonstrate the design of shunt-starting networks. Parallelly, an important step is the study of the selection of the phase implemented by the extra input element of the double element solution. Two solutions of B_{S1} are found and they will both conduct to two different solutions and so, it is interesting to assess which one yields better elements in terms of acoustic technology limitations.

Additionally, defining specific search rules for networks starting in shunt is of interest to boost the application of the synthesis tool to an automated search engine capable of finding the better solution for a given set of filter specifications.

Appendix A

A.1 Polynomial Para-conjugation

Consider an N-th degree polynomial $Q(s)$ on $s = j\omega$ and complex coefficients q_i for $i = 0,\ 1,\ 2, ...,\ N$. Then, operation $Q(s)^*$ is equivalent to $Q^*(-s)$. That is conjugating coefficients and changing sign on variable s. For example,

$$\begin{aligned} Q(s)^* = Q^*(-s) &= q_0^* - q_1^* s + q_2^* s^2 + ... + q_N^* s^N \text{for } N \text{ even} \\ Q(s)^* = Q^*(-s) &= q_0^* - q_1^* s + q_2^* s^2 + ... - q_N^* s^N \text{for } N \text{ odd} \end{aligned} \tag{A.1}$$

As the conjugation operation, noted $Q^*(s)$ reflects the roots of $Q(s)$ about the real axis, the para-conjugation operation, namely $Q(s)^*$ reflects the roots of $Q(s)$ about the imaginary axis. If the N complex-plane roots of $Q(s)$ are r_k, for $k = 0,\ 1,\ 2, ...,\ N$, then the para-conjugated roots will be $-r_k^*$. Then, during the construction of $Q(s)^*$ from the para-conjugated roots, term $(-1)^N$ must multiply the resulting polynomial to ensure the correct sign of the leading coefficient.

$$Q(s)^* = Q^*(-s) = (-1)^N \prod_{k=1}^{N} (s + r_k^*)$$

A.2 ABCD Polynomials

A two-port network connected between unitary terminations can be expressed in terms of the [ABCD] matrix as

$$[ABCD] = \frac{1}{jP(s)/\varepsilon} \begin{bmatrix} A(s) & B(s) \\ C(s) & D(s) \end{bmatrix}$$

where polynomials $A(s)$, $B(s)$, $C(s)$ and $D(s)$ are closely related to the coefficients of characteristic polynomials $E(s)$ and $F(s)/\varepsilon_r$.

In [20], the following expressions are outlined to construct the [ABCD] polynomials for networks that might include FIRs.

$$A(s) = j\text{Im}(e_0 + f_0) + \text{Re}(e_1 + f_1)s + j\text{Im}(e_2 + f_2)s^2 + \cdots + j\text{Im}(e_N + f_N)s^N \tag{A.2a}$$

$$B(s) = \text{Re}(e_0 + f_0) + j\text{Im}(e_1 + f_1)s + \text{Re}(e_2 + f_2)s^2 + \cdots + \text{Re}(e_N + f_N)s^N \tag{A.2b}$$

$$C(s) = \text{Re}(e_0 - f_0) + j\text{Im}(e_1 - f_1)s + \text{Re}(e_2 - f_2)s^2 + \cdots + \text{Re}(e_N - f_N)s^N \tag{A.2c}$$

$$D(s) = j\text{Im}(e_0 - f_0) + \text{Re}(e_1 - f_1)s + j\text{Im}(e_2 - f_2)s^2 + \cdots + j\text{Im}(e_N - f_N)s^N \tag{A.2d}$$

for N even, and

$$A(s) = \text{Re}(e_0 + f_0) + j\text{Im}(e_1 + f_1)s + \text{Re}(e_2 + f_2)s^2 + \cdots + \text{Re}(e_N + f_N)s^N \tag{A.3a}$$

$$B(s) = j\text{Im}(e_0 + f_0) + \text{Re}(e_1 + f_1)s + j\text{Im}(e_2 + f_2)s^2 + \cdots + j\text{Im}(e_N + f_N)s^N \tag{A.3b}$$

$$C(s) = j\text{Im}(e_0 - f_0) + \text{Re}(e_1 - f_1)s + j\text{Im}(e_2 - f_2)s^2 + \cdots + j\text{Im}(e_N - f_N)s^N \tag{A.3c}$$

$$D(s) = \text{Re}(e_0 - f_0) + j\text{Im}(e_1 - f_1)s + \text{Re}(e_2 - f_2)s^2 + \cdots + \text{Re}(e_N - f_N)s^N \tag{A.3d}$$

for N odd.

Bibliography

[1] R. Ruby, P. Bradley, Y. Oshmyansky, A. Chien, and J. Larson, "Thin film bulk wave acoustic resonators (FBAR) for wireless applications," in *2001 IEEE Ultrasonics Symposium. Proceedings. An International Symposium (Cat. No.01CH37263)*. IEEE, 2001.

[2] T. Makkonen, T. Pensala, J. Vartiainen, J. Knuuttila, J. Kaitila, and M. Salomaa, "Estimating materials parameters in thin-film BAW resonators using measured dispersion curves," *IEEE Transactions on Ultrasonics, Ferroelectrics and Frequency Control*, vol. 51, no. 1, pp. 42–51, jan 2004.

[3] A. R. Giménez, "Rf filters and multiplexers based on acoustic wave technologies with ladder-type and cross-coupled topologies. designing under a systematic strategy," Ph.D. dissertation, Universitat Autònoma de Barcelona, 2016.

[4] P. Warder and A. Link, "Golden age for filter design: Innovative and proven approaches for acoustic filter, duplexer, and multiplexer design," *IEEE Microwave Magazine*, vol. 16, no. 7, pp. 60–72, aug 2015.

[5] G. G. Fattinger, A. Volatier, M. Al-Joumayly, Y. Yusuf, R. Aigner, N. Khlat, and M. Granger-Jones, "Carrier aggregation and its challenges - or: The golden age for acoustic filters," in *2016 IEEE MTT-S International Microwave Symposium (IMS)*. IEEE, may 2016.

[6] M. Cooper, R. W. Dronsuth, A. J. Leitich, J. C. N. Lynk, J. J. Mikulski, J. F. Mitchell, R. A. Richardson, and J. H. Sangster, "Radio telephone system," U.S. Patent US3 906 166A, 1973.

[7] D. P. Morgan, "History of saw devices," in *Proceedings of the 1998 IEEE International Frequency Control Symposium (Cat. No.98CH36165)*, May 1998, pp. 439–460.

[8] K. Lakin, J. Wang, G. Kline, A. Landin, Y. Chen, and J. Hunt, "Thin film resonators and filters," in *1982 Ultrasonics Symposium*. IEEE, 1982.

[9] R. Ruby, P. Bradley, J. Larson, and Y. Oshmyansky, "PCS 1900 MHz duplexer using thin film bulk acoustic resonators (FBARs)," *Electronics Letters*, vol. 35, no. 10, p. 794, 1999.

[10] K. Hashimoto, *RF Bulk Acoustic Wave Filters for Communications*, ser. Artech House microwave library. Artech House, 2009.

[11] R. Ruby, "A snapshot in time: The future in filters for cell phones," *IEEE Microwave Magazine*, vol. 16, no. 7, pp. 46–59, aug 2015.

[12] T. Bauer, C. Eggs, K. Wagner, and P. Hagn, "A bright outlook for acoustic filtering: A new generation of very low-profile SAW, TC SAW, and BAW devices for module integration," *IEEE Microwave Magazine*, vol. 16, no. 7, pp. 73–81, aug 2015.

[13] J. Verdú, "Bulk acoustic wave resonators and their application to microwave devices," Ph.D. dissertation, Universitat Autònoma de Barcelona, 2010.

[14] H. Campanella, *Acoustic Wave and Electromechanical Resonators: Concept to Key Applications*, ser. Artech House integrated microsystems series. Artech House, 2010.

[15] J. Larson, P. Bradley, S. Wartenberg, and R. Ruby, "Modified butterworth-van dyke circuit for FBAR resonators and automated measurement system," in *2000 IEEE Ultrasonics Symposium. Proceedings. An International Symposium (Cat. No.00CH37121)*. IEEE, 2000.

[16] W. P. Mason and H. Baerwald, "Piezoelectric crystals and their applications to ultrasonics," *Physics Today*, vol. 4, no. 5, pp. 23–24, may 1951.

[17] G. Kovacs, "A generalised p-matrix model for SAW filters," in *IEEE Symposium on Ultrasonics, 2003.* IEEE, 2003.

[18] A. Triano, P. Silveira, J. Verdu, and P. de Paco, "Synthesis methodology for mixed-topology acoustic wave filters," in *2019 IEEE International Ultrasonics Symposium (IUS)*. IEEE, oct 2019.

[19] M. Jimenez Blasco, "A coupling matrix vision for mobile filtering devices with micro-acoustic wave technologies. a systematic approach," Ph.D. dissertation, Universitat Autònoma de Barcelona, 2015.

[20] R. J. Cameron, C. M. Kudsia, and R. R. Mansour, *Microwave Filters for Communication Systems*. John Wiley & Sons, 2018.

[21] A. Atia and A. Williams, "Narrow-bandpass waveguide filters," *IEEE Transactions on Microwave Theory and Techniques*, vol. 20, no. 4, pp. 258–265, apr 1972.

[22] S. Amari and G. Macchiarella, "Synthesis of inline filters with arbitrarily placed attenuation poles by using nonresonating nodes," *IEEE Transactions on Microwave Theory and Techniques*, vol. 53, no. 10, pp. 3075–3081, oct 2005.

[23] S. Tamiazzo and G. Macchiarella, "Synthesis of cross-coupled prototype filters including resonant and non-resonant nodes," *IEEE Transactions on Microwave Theory and Techniques*, vol. 63, no. 10, pp. 3408–3415, oct 2015.

[24] R. Baum, "Design of unsymmetrical band-pass filters," *IRE Transactions on Circuit Theory*, vol. 4, no. 2, pp. 33–40, 1957.

[25] D. M. Pozar, *Microwave Engineering*. John Wiley & Sons Inc, 2011.

[26] R. M. Foster, "A reactance theorem," *Bell System Technical Journal*, vol. 3, no. 2, pp. 259–267, apr 1924.

[27] S. Amari and U. Rosenberg, "New building blocks for modular design of elliptic and self-equalized filters," *IEEE Transactions on Microwave Theory and Techniques*, vol. 52, no. 2, pp. 721–736, feb 2004.

[28] A. Gimenez, J. Verdu, and P. de Paco, "General synthesis methodology for the design of acoustic wave ladder filters and duplexers," *IEEE Access*, vol. 6, pp. 47 969–47 979, 2018.

[29] A. Triano, J. Verdu, P. de Paco, T. Bauer, and K. Wagner, "Relation between electromagnetic coupling effects and network synthesis for acoustic wave ladder type filters," in *2017 IEEE International Ultrasonics Symposium (IUS)*. IEEE, sep 2017.